Received: 2 July 2021 | Revised: 22 November 2021 | Accepted: 22 December 2021

DOI: 10.1002/jev2.12184

RESEARCH ARTICLE

Optimization of small extracellular vesicle isolation from expressed prostatic secretions in urine for in-depth proteomic analysis

Vanessa L. Correll[1] | **Joseph J. Otto**[1] | **Cristina M. Risi**[2] | **Brian P. Main**[1] | **Paul C. Boutros**[3,4,5,6,7,8] | **Thomas Kislinger**[3,9] | **Vitold E. Galkin**[2] | **Julius O. Nyalwidhe**[1,10] | **O. John Semmes**[1,10] | **Lifang Yang**[1,10]

[1] Leroy T. Canoles Jr. Cancer Research Center, Eastern Virginia Medical School, Norfolk, Virginia, USA

[2] Department of Physiological Sciences, Eastern Virginia Medical School, Norfolk, Virginia, USA

[3] Department of Medical Biophysics, University of Toronto, Toronto, Canada

[4] Department of Pharmacology and Toxicology, University of Toronto, Toronto, Canada

[5] Department of Human Genetics, University of California, Los Angeles, California, USA

[6] Department of Urology, University of California, Los Angeles, California, USA

[7] Institute for Precision Health, University of California, Los Angeles, California, USA

[8] Jonsson Comprehensive Cancer Center, University of California, Los Angeles, California, USA

[9] Princess Margaret Cancer Centre, University Health Network, Toronto, Canada

[10] Department of Microbiology and Molecular Cell Biology, Eastern Virginia Medical School, Norfolk, Virginia, USA

Correspondence
Lifang Yang, Ph.D., Eastern Virginia Medical School, 651 Colley Ave., Norfolk, VA 23501, USA.
Email: yanglf@evms.edu

Funding information
National Cancer Institute, Grant/Award Number: U01CA214194

Abstract

The isolation and subsequent molecular analysis of extracellular vesicles (EVs) derived from patient samples is a widely used strategy to understand vesicle biology and to facilitate biomarker discovery. Expressed prostatic secretions in urine are a tumor proximal fluid that has received significant attention as a source of potential prostate cancer (PCa) biomarkers for use in liquid biopsy protocols. Standard EV isolation methods like differential ultracentrifugation (dUC) co-isolate protein contaminants that mask lower-abundance proteins in typical mass spectrometry (MS) protocols. Further complicating the analysis of expressed prostatic secretions, uromodulin, also known as Tamm-Horsfall protein (THP), is present at high concentrations in urine. THP can form polymers that entrap EVs during purification, reducing yield. Disruption of THP polymer networks with dithiothreitol (DTT) can release trapped EVs, but smaller THP fibres co-isolate with EVs during subsequent ultracentrifugation. To resolve these challenges, we describe here a dUC method that incorporates THP polymer reduction and alkaline washing to improve EV isolation and deplete both THP and other common protein contaminants. When applied to human expressed prostatic secretions in urine, we achieved relative enrichment of known prostate and prostate cancer-associated EV-resident proteins. Our approach provides a promising strategy for global proteomic analyses of urinary EVs.

KEYWORDS

biomarkers, EPS-urine, expressed prostatic secretions in urine, extracellular vesicle, mass spectrometry, prostate cancer, proteomics, Tamm-Horsfall protein, urine, uromodulin

1 | INTRODUCTION

Prostate cancer (PCa) is the most common cancer and the second leading cause of cancer death among men in the United States (Siegel et al., 2021). It exhibits highly heterogeneous clinical behaviour, with newly diagnosed cases ranging from inherently indolent diseases amenable to active surveillance to aggressive malignancies that are lethal if untreated (Litwin &

Tan, 2017). There is therefore a critical unmet need for the development of biomarkers to accurately quantify the metastatic potential of newly diagnosed or untreated tumours. Ideal biomarkers would be detectable through a "liquid biopsy" technique which facilitates minimally invasive or non-invasive surveillance of disease status to support safe active surveillance of men with highly indolent disease. Monitoring of prostate-specific antigen (PSA) concentration is widely used for this purpose but has insufficient specificity and sensitivity for PCa when used alone or in combination with other molecular biomarkers (Duffy, 2020).

Expressed prostatic secretions in urine (EPS-urine) provide a promising avenue to fill this gap. EPS-urine can be obtained by collecting urine after a clinical standard-of-care digital rectal exam (DRE) (Drake et al., 2009). This fluid is enriched with prostate-derived proteins and represents a readily available source for prostate-specific biomarkers (Y. Kim et al., 2016; Principe et al., 2012). We and other groups have demonstrated that EPS-urine is also enriched with extracellular vesicles (EVs) derived from the prostate and urinary tract (Principe et al., 2013). These small membrane-enclosed vesicles include "exosomes" (~40–150 nm) which are released by surface fusion of endosome-derived multivesicular bodies and other similarly sized EVs depending upon the isolation technique employed (Kowal et al., 2014; Raposo & Stoorvogel, 2013; Théry et al., 2018). As a result of the mechanics of EV biogenesis, the molecular content of EVs is heavily influenced by that of the parent cell. Importantly, EVs mediate intracellular communication by transferring bioactive cargo molecules including nucleic acids, lipids, and proteins to target cells at local or distal sites (Raposo & Stoorvogel, 2013; Théry et al., 2018). Tumour-derived EVs function in tumorigenesis and progression by interacting with the tumour microenvironment (Becker et al., 2016). Moreover, the presence of the bilayer membrane shelters enclosed cargo molecules from exogenous nucleases, proteases, and other degradative enzymes, ensuring the high stability of EVs in different kinds of body fluids including urine. Thousands of proteins have been identified in these vesicles in recent proteomic studies (Rosa-Fernandes et al., 2017). Therefore, protein profiling of urinary extracellular vesicles (uEVs) derived from EPS-urine of PCa patients holds promise for the development of non-invasive PCa biomarkers to assist clinical management of this disease (Duijvesz et al., 2011, Nawaz et al., 2014).

Although a highly desirable source for protein biomarkers, there are substantial challenges inherent to isolating EVs from urine (Erdbrügger et al., 2021). Urine possesses a wide ionic concentration and pH range, a dynamic magnitude of protein abundance, and high intra- and inter-individual variability (Decramer et al., 2008; Jeon et al., 2020; Oeyen et al., 2019; X. Xu, et al., 2019). Additionally, the presence of large amounts of uromodulin, also known as Tamm-Horsfall protein (THP), poses a unique problem for uEV isolation. THP is normally the most abundant protein in urine, with 30–60 mg secreted each day (Micanovic et al., 2020). It is synthesized as a GPI-linked membrane glycoprotein that is secreted into the urine after extracellular proteolytic cleavage (Micanovic et al., 2020). Secreted THP monomers aggregate to form high molecular weight ropelike filaments or matrices visible with electron microscopy (Micanovic et al., 2020; Wiggins, 1987; Wu et al., 2018). These THP matrices can trap EVs making them unavailable for analysis, reducing yields (Fernández-Llama et al., 2010; Wachalska et al., 2016). Secondly, like other contaminating soluble proteins, THP monomers/oligomers can concomitantly sediment with and/or bind to EVs, reducing final uEV purity (Musante et al., 2012; X. Xu et al., 2019). Together, these two factors skew uEV recovery and reduce the depth of detection of low-abundance uEV proteins by mass spectrometry (MS) analysis (Hiemstra et al., 2011).

Several strategies have been employed to minimize the impact of THP on uEV yield and purity. Differential ultracentrifugation (dUC) is the most widely used method to isolate EVs (Dhondt et al., 2018; Gardiner et al., 2016; Royo et al., 2020). Conventional dUC employs consecutive centrifugation steps in which an early "low-speed" (17,000–20,000 g) centrifugation removes larger THP matrices. However, a portion of the uEV population co-separates with the THP matrix, reducing recovery and introducing bias (Fernández-Llama et al., 2010). Treatment of the low-speed pellet with the reducing agent dithiothreitol (DTT) depolymerizes THP and enables recovery of trapped-EVs (Fernández-Llama et al., 2010). Unfortunately, smaller THP fibres, generated during depolymerization, represent a significant source of potential contamination and co-sediment with EVs during subsequent "high-speed" (100,000–200,000 g) centrifugation steps (Musante et al., 2012; X. Xu, et al., 2019). In this report, we described an improved dUC method that employs an alkaline wash to effectively recover THP-entrapped uEVs while reducing contaminating proteins. The approach resulted in significant improvement of both the yield and purity of uEVs when compared to existing dUC methodologies. As a biological challenge for the new methodology, we applied our protocol to EPS-urine samples from PCa patients and describe a PCa-associated uEVs proteome using MS.

2 | MATERIALS AND METHODS

2.1 | Patient EPS-urine collection

Samples were obtained from patients following informed consent and use of Institutional Review Board-approved protocols at Eastern Virginia Medical School and Urology of Virginia. EPS-urine was collected as previously described (Drake et al., 2009). Briefly, a DRE was performed in which each lobe of the prostate was gently stroked three times to force prostatic fluid into the urethra. Then, a urine sample containing EPS-urine was collected. Samples were transported to the biorepository on ice, and unprocessed EPS-urine was stored at -80°C and later used to generate EPS-urine pools for EV isolation.

2.2 | Generation of EPS-urine pools

Two pools (pool 1–15 patients, pool 2–10 patients) were made from EPS-urine from men (average age at sample collection – 65.7 years) diagnosed with low- to intermediate-risk disease based upon National Comprehensive Cancer Network (NCCN) risk groups. Clinical information is summarized in Supplementary Table S1. Unprocessed EPS-urine was thawed overnight at 4°C, and 20 ml from each patient was combined to generate a pool which was mixed, aliquoted, and stored at -80°C. Pool 1 was used for all experiments (Figures 1–8), and pool 2 was used for two of three replicates described in Figure 2.

2.3 | Isolation of EVs from EPS-urine

We developed methodological improvements upon a previously described dUC approach which included DTT-mediated recovery of THP-entrapped EVs (Fernández-Llama et al., 2010). Aliquots (18 ml) of pooled EPS-urine were thawed overnight (~16 h) at 4°C. Samples were vortexed vigorously for 1 min to disperse EV clusters (Zhou et al., 2006). The EPS-urine was then transferred to Beckman 363647 tubes and centrifuged at 20,000 g (20,001 RCF_{max}; 12,859 RPM) for 30 min in a fixed-angle rotor (JA-20, adjusted k-factor 1863.4) to remove cells and cell debris. The 20,000 g supernatant (SN1) was kept on ice during subsequent processing of the 20,000 g pellet (P1). P1 was resuspended in isolation buffer (IS buffer: 0.25 M sucrose, 10 mM HEPES, 1 mM EDTA, pH 7.4) and an equal volume of freshly prepared DTT (400 mg/ml in IS Buffer) was added to achieve a final concentration of 200 mg/ml DTT. Resuspended P1 was vortexed, incubated at 37°C for 5 min, vortexed, and incubated for an additional 5 min. The DTT-treated P1 was centrifuged at 20,000*g* (19,910 RCF_{max}; 12,800 RPM) for 30 min in a thick-walled centrifuge tube in a swinging-bucket rotor (SW55Ti, adjusted k-factor 895.4). The resulting supernatant (SN2), containing EVs released from the THP matrix, was combined with the cell-free EPS-urine (SN1) in Beckman 326823 tubes. The tubes were topped off with phosphate-buffered saline (PBS) and were ultracentrifuged at 175,000*g* (174,899 RCF_{max}; 32,000 RPM) for 2 h in a swinging-bucket rotor (SW32 Ti, k-factor 204.2). The resulting pellet (P3) was washed by resuspension in 5 ml of chilled freshly prepared alkaline solution (150 mM Na_2CO_3 pH 11.0) and was passed through a 0.22 μM PES syringe filter (Millipore SLGP033RS) to remove large particles. The filter was rinsed with an additional 5 ml of alkaline solution, and the total filtrate was transferred to Beckman 331374 tubes. The tube volume was topped off with alkaline solution, and the sample was ultracentrifuged again at 175,000 g (175,359 RCF_{max}; 31,400 RPM) for 2 h and 10 min in a SW40Ti swinging-bucket rotor (SW40Ti, adjusted k-factor 222.9). A Beckman Avanti J-E centrifuge was used for the initial centrifugation step and subsequent spins were conducted in a Beckman Optima XL-100K or Optima XPN-100 ultracentrifuge. All spins were performed at 4°C with maximum acceleration and deceleration settings applied.

In our comparison studies, we used PBS instead of the prepared alkaline solution. Therefore, we referred to these methods as DTT-PBS and DTT-ALK. For both methods, the resulting final EV pellet (P4) was resuspended in ~100–200 μl cold PBS and was stored in a microcentrifuge tube.

For methods that did not include a step to recover the THP matrix-bound EVs, we eliminated the DTT incubation step. As a comparison, we incorporated either an alkaline wash (ALK method) or PBS wash (PBS method) (Øverbye et al., 2015) of the 175,000 g pellet (P3), respectively. A diagram of the DTT-ALK, DTT-PBS, ALK, and PBS methods is shown in Figure 1a-b.

For experiments involving the separate isolation of SN1-derived and SN2-derived EVs, the DTT-ALK method was performed, but the cell-free EPS-urine (SN1) and the 20,000 g supernatant from the DTT treatment (SN2) were not combined prior to the first 175,000 g spin. A schematic of the methodology is in Figure 3a.

2.4 | Nanoparticle tracking analysis (NTA)

The size distribution and concentration of the particles in the resuspended 175,000 g EV pellet (P4) were determined by NTA with a NanoSight NS300 instrument (Malvern) equipped with a 488 nm laser and a sCMOS camera. NTA software version 3.3 (Malvern) was used for data acquisition and analysis. Samples were diluted in PBS to achieve a particle concentration within the optimal range for analysis reported by the manufacturer. Samples were manually injected with a syringe, and five 60-second videos (technical replicates) were captured and analyzed with the following settings: camera level 14, temperature 25°C, and viscosity 0.9 cP (water). For analysis, a detection threshold of five was used, and blur size and max jump distance were set to automatic.

2.5 | Transmission electron microscopy (TEM)

Aliquots of the resuspended 175,000 g EV pellets (P4) in PBS were further diluted in PBS to achieve an optimal concentration based upon NTA results. A small volume of the diluted EVs was incubated for 30 s on carbon-coated, glow discharged grids

(Electron Microscopy Sciences, FCF300-Cu-SB). After negative staining with 2% (w/v) uranyl acetate, a JEM-1200EX (JEOL) Transmission Electron Microscope was used at an accelerating voltage of 70 kV to record micrographs at nominal magnifications of 15,000× and 30,000×. The electron microscope operator was blinded to the experimental condition of the samples during image acquisition.

2.6 | Protein content assay

For EV lysis and protein extraction, an aliquot of the resuspended EVs in PBS was solubilized in RIPA buffer. Samples were sonicated twice in a water bath for 5 min at room temperature and were placed on ice for 5 min between each sonication. The total protein content of RIPA extracts was quantified by a micro bicinchoninic acid (BCA) assay (Thermo Fisher 23235).

2.7 | Western blotting

For SDS-PAGE, a volume of EVs corresponding to 1.5 μg of total protein was prepared in Laemmli sample buffer (BioRad 1610747) containing β-mercaptoethanol and heated at 95°C for 5 minutes. Proteins were separated through a 4%–12% NuPAGE Bis-Tris gel (Invitrogen), transferred to an Immobilon-FL PVDF membrane (Millipore), and detected as described previously (Yang et al., 2011). After blocking with Intercept blocking buffer (Licor Biosciences), the following antibodies were used: mouse anti-calnexin (BD Biosciences 610523, 1:500), rabbit anti-GM130 (Abcam ab52649, 1:500), mouse anti-cytochrome c (BD Biosciences 556433, 1:1000), rabbit anti-CD9 (Cell Signaling Technologies 13174, 1:1000), mouse anti-TSG101 (BD Biosciences 612696, 1:500), and mouse anti-THP (Santa Cruz Biotechnology sc-271022, 1:1000), rabbit anti-beta-actin (Invitrogen, PA1-16889, 1:5000), donkey anti-mouse IgG IRDye 800CW (LiCor 925–32212, 1:10,000), and donkey anti-rabbit IgG IRDye 680RD (LiCor 926–68073, 1:10,000).

2.8 | Sample preparation for LC-MS/MS

EVs in PBS (15 μg protein) were concentrated in a SpeedVac (Thermo Fisher Scientific) to ~20 μl and prepared in Laemmli sample buffer (BioRad 1610747) containing 10 mM DTT. Samples were loaded into a 4%–12% NuPAGE Bis-Tris gel (Invitrogen) and were run until samples travelled 2 cm in the gel. In-gel digestion was performed as previously described (Yang et al., 2015). Peptides were extracted with 50% acetonitrile/0.1% formic acid, dried in a SpeedVac, resuspended in 0.1% formic acid, and quantified with a NanoDrop One spectrophotometer (Thermo Fisher Scientific, 205 nm).

2.9 | Protein identification by LC-MS/MS

Tryptic peptides were analyzed on an Orbitrap Fusion Lumos mass spectrometer coupled to an EASY nLC 1200 nano-flow UHPLC system (Thermo Fisher). For each injection, 2 μg of peptides were loaded onto a 2 cm C18 pre-column (75 μM diameter, 3 μM particle size, 100 Å pore size, Thermo Fisher 164946) before elution into a 50 cm analytical C18 column (75 μM diameter, 2 μM particle size, 100 Å pore size, Thermo Fisher ES803A). LC solvents consisted of 0.1% (v/v) formic acid/water as buffer A and 0.1% (v/v) formic acid in 80% acetonitrile as buffer B. Peptides were separated using a 140-min stepped linear gradient with 250 nl/min flow rate: 8%–12% B for 5 min, 12%–30% B for 100 min, 30%–60% B for 20 min, 60%–98% B for 5 min, hold 98% B for 10 min. Injections were performed in triplicate to yield three technical replicates per sample. At least two blank injections of buffer A (30-min method) were included between sample injections to minimize sample carryover between consecutive runs. Data were acquired in data-dependent acquisition mode (DDA). MS1 data detection was performed in the Orbitrap under the following conditions: Resolution 120K, scan range (m/z) = 375–1500, maximum injection time 50 ms, and automatic gain control (AGC) of 4×10^5. Precursor ions for MS2 scans were isolated in the quadrupole with a 1.6 m/z window and fragmented by HCD with a 35% collision energy prior to detection in the Ion Trap with a maximum injection time of 35 ms and an AGC of 1×10^4. Raw files were searched using MaxQuant software (version 1.6.1.0) against a human Swiss-Prot database (20,215 entries, canonical database) (Cox & Mann, 2008; Cox et al., 2011). Oxidation of methionine and N-terminal protein acetylation were included as variable modifications, and carbamidomethylation of cysteine was set as a fixed modification. The first search peptide tolerance was set to 20 ppm, and the main search peptide tolerance was set to 10 ppm. Trypsin was selected as the enzyme and a maximum of two missed cleavages were allowed. The minimum peptide length was set to seven amino acids. The match between runs feature was enabled with default settings (match time window of 0.7 min and alignment time of 20 min). MaxQuant's label-free quantification (LFQ) algorithm was enabled for the calculation of LFQ intensities, and the LFQ minimum ratio count was set

to 2. False discovery rates (FDR) for peptide spectral matches (PSM) and protein identifications were set to 0.01 (1%). Default settings were used for the remaining options.

2.10 | Proteomic data analysis

Perseus software (version 1.6.2.2) was used for proteomic data statistical analysis (Tyanova & Cox, 2018). The MaxQuant proteingroups.txt file was imported, and potential contaminants, reverse database hits, proteins only identified by site, and protein groups with fewer than two unique peptide identifications across raw files were removed. LFQ intensities of zero (missing values) were converted to NaN, and protein groups with at least two valid values (i.e., detection in at least two of three technical replicates) in at least one condition were selected. After this initial filtering, LFQ intensities were $\log_2$ transformed, and missing values were imputed with numbers drawn from normal distribution and simulating low-abundance measurements (default parameters: 0.3 width, 1.8 standard deviation down shift, separately for each column). Principal component analysis (PCA) and one-way analysis of variance (ANOVA) were performed after the imputation step. ANOVA was conducted with the following settings available in Perseus: permutation-based FDR threshold set to 0.05 and S0 parameter (artificial within groups variance) set to 2. Heatmaps with hierarchical clustering of z-score normalized $\log_2$(LFQ intensities) were generated in Perseus (using default parameters). The average $\log_2$(LFQ intensity) of technical replicates, calculated prior to missing value imputation, was used to determine protein group rank and quartile within each condition. All other statistical analyses mentioned in this report were conducted with GraphPad Prism software.

2.11 | Bioinformatic analysis

Functional enrichment analyses were performed using g:Profiler against a background of the *H. sapiens* proteome and default parameters (Raudvere et al., 2019). Enrichment of Gene Ontology (GO) terms was considered statistically significant when corrected for multiple testing by the g:SCS method with adjusted $p < 0.05$. Cytoscape and the EnrichmentMap pipeline were used to visualize enriched GO terms, as described previously (Reimand et al., 2019). Tissue distribution analysis was performed using g:Profiler against Human Protein Atlas (HPA) normal tissue database (https://www.proteinatlas.org/humanproteome/tissue, version 2019-12-17), where the protein expression data is derived from antibody-based protein profiling 57 normal human tissue types using immunohistochemistry, and the one with the reliability scores of enhanced, supported, and approved was extracted for the analysis (Reimand et al., 2019; Uhlén et al., 2015). The PCa signalling pathway was generated through the use of commercially available curated database software Ingenuity Pathway Analysis (IPA).

2.12 | Data availability

We have submitted all relevant data of our experiments to the EV-TRACK knowledgebase (EV-TRACK ID: EV210199; EV-METRIC: 78%) (Van Deun et al., 2017). The mass spectrometry proteomics data have been deposited to the ProteomeXchange Consortium via the PRIDE (Perez-Riverol et al., 2019) partner repository with the dataset identifier PXD026974.

3 | RESULTS

3.1 | Comparison of uEVs isolated from optimized differential ultracentrifugation strategies

Previous studies showed that reducing agents can efficiently depolymerize the THP matrix in the low-speed pellet to release THP-entrapped urinary EVs (Fernández-Llama et al., 2010). However, THP oligomers/monomers and other abundant proteins can co-pellet with EVs during subsequent high-speed ultracentrifugation (UC) (Musante et al., 2012; X. Xu, et al., 2019). Alternatively, the THP depolymerization step can be bypassed to avoid these contaminants (Pisitkun et al., 2004; Théry et al., 2006), with a concomitant loss of a portion of urine EVs (Fernández-Llama et al., 2010). Sodium carbonate washes have been used to discriminate between integral and peripheral membrane proteins (Fujiki, Fowler, et al., 1982; Fujiki, Hubbard, et al., 1982). We reasoned that introduction of an alkaline sodium carbonate wash could improve EV purity by changing the protonation states of ionizable groups of EVs and their binding proteins, thereby reducing non-covalent interactions. We evaluated the effectiveness of the alkaline wash step by comparing four methods for uEV isolation: (1) DTT treatment of the low-speed pellet (20,000 g) and alkaline wash of the high-speed pellet (175,000 g); (2) DTT treatment of the low speed-pellet and PBS wash of the high-speed pellet; (3) bypassing DTT treatment of the low-speed pellet and employing an alkaline wash of the high-speed pellet; and (4) bypassing DTT treatment of the low-speed pellet and employing a PBS wash of the high-speed pellet. The four approaches are

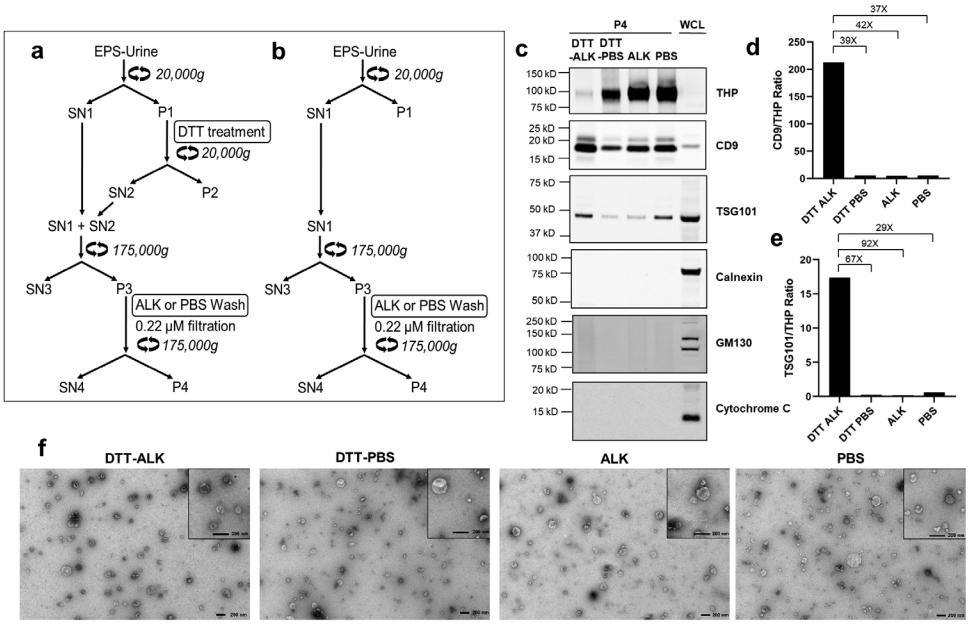

FIGURE 1 Characterization of EPS-urine extracellular vesicles enriched by differential ultracentrifugation (dUC). **a-b,** A schematic overview of four dUC-based methods for isolation of EPS-urine EVs : (a) Two approaches employed a depolymerization of THP matrix by DTT treatment of the 20,000 g pellet followed by a subsequent PBS (DTT-PBS method) or alkaline (DTT-ALK method) wash step; (b) An additional two approaches were compared that did not include a THP depolymerization step and either included a PBS or ALK wash step of the 175,000 g pellet. Primary and subsequent supernatant (SN) and pellet (P) fractions are noted. For all approaches, a 0.22 μm filtration step was applied between two ultracentrifugations. **c-e,** Western blot analysis of EVs enriched through each approach. (c) The blot was probed with antibodies against Tamm-Horsfall protein (THP), EV-markers CD9 and TSG101, endoplasmic reticulum marker (calnexin), Golgi marker (GM130), and mitochondrial marker (cytochrome C). 1.5 μg of the P4 EV fractions were loaded in each lane. 45 μg of whole-cell lysate (WCL) from the DU145 prostate cancer cell line was included as a negative control for THP and as a positive control for calnexin, GM130, and cytochrome c. Densitometry analysis of the western blot showing the ratio of the integrated band intensities (K counts) of (d) EV-markers CD9 and (e) TSG101 versus THP. The fold change is indicated. **f,** TEM micrographs of the P4 fractions. Magnifications of 15,000× and 30,000× (inserts) are shown. Scale bar = 200 nm.

referred to as DTT-ALK, DTT-PBS, ALK, and PBS, respectively. For all methods, we incorporated a 0.22 μm filtration step to enrich for small uEVs while excluding larger particles. A schematic of the dUC approaches is shown in Figure 1a,b.

Since there are significant variations in urine proteome and EV content, we used pooled EPS-urine samples from a patient cohort for the optimization of uEV isolation. For this study, two pools (pool 1 $n = 15$, pool 2 $n = 10$) were made from EPS-urine of men diagnosed with NCCN low- to intermediate-risk disease (clinical Gleason score of 6 or 7 and clinical staging of T1c, T2a, or T2b). Clinical information about each sample is in Supplementary Table S1. We demonstrated the overall variability in the urine proteome by total protein assay, SDS-PAGE, and western blot analysis of the individual samples comprising the resulting pools (Supplementary Figure S1).

The uEVs preparations were evaluated by western blot for the relative abundance of the EV-specific markers CD9 and TSG101. Western blot analysis demonstrated that, when normalized to total protein, higher levels of CD9 and TSG101 were detected in uEV lysate from the DTT-ALK method (Figure 1c). By contrast, contaminating THP was dramatically reduced in the uEV prepared by DTT-ALK relative to other methods. Quantitation by secondary densitometry confirmed that DTT-ALK uEVs were enriched for CD9 and TSG101 relative to THP (Figure 1d,e). The DTT-ALK approach resulted in 37–42 fold greater CD9/THP ratio and a 29–92 fold greater TSG101/THP ratio compared to DTT-PBS, ALK, and PBS. The markers for endoplasmic reticulum (calnexin), Golgi (GM130), and mitochondria (cytochrome c) were undetected in all EV preparations but were observed in the whole-cell lysate of DU145 cells which served as a positive control. We also conducted a morphological characterization of the uEVs using TEM. All uEV preparations harboured heterogeneously-sized particles with characteristic round-shaped vesicular structure (Figure 1f). Importantly, uEVs isolated under alkaline conditions (DTT-ALK and ALK) showed intact membrane-encapsulated vesicles indicating that the alkaline wash does not disturb the structural integrity of uEVs. Considering the limited improvement in uEV enrichment via the ALK method when compared to the PBS method (Figure 1c) and the absence of the depolymerization step to access THP-integrated EVs, we decided to exclude the ALK method from further analysis.

We employed nanoparticle tracking analysis (NTA) to determine the size distribution and particle yield of uEVs isolated by the DTT-ALK, DTT-PBS, and PBS approaches. All methods enriched small particles, mainly between 50 and 150 nm, which were within the expected size-range for small EVs (Figure 2a-f). The mean and mode size of particles isolated by the DTT-ALK and PBS method were not significantly different (Figure 2e,f). However, DTT-ALK and PBS displayed tighter size distributions

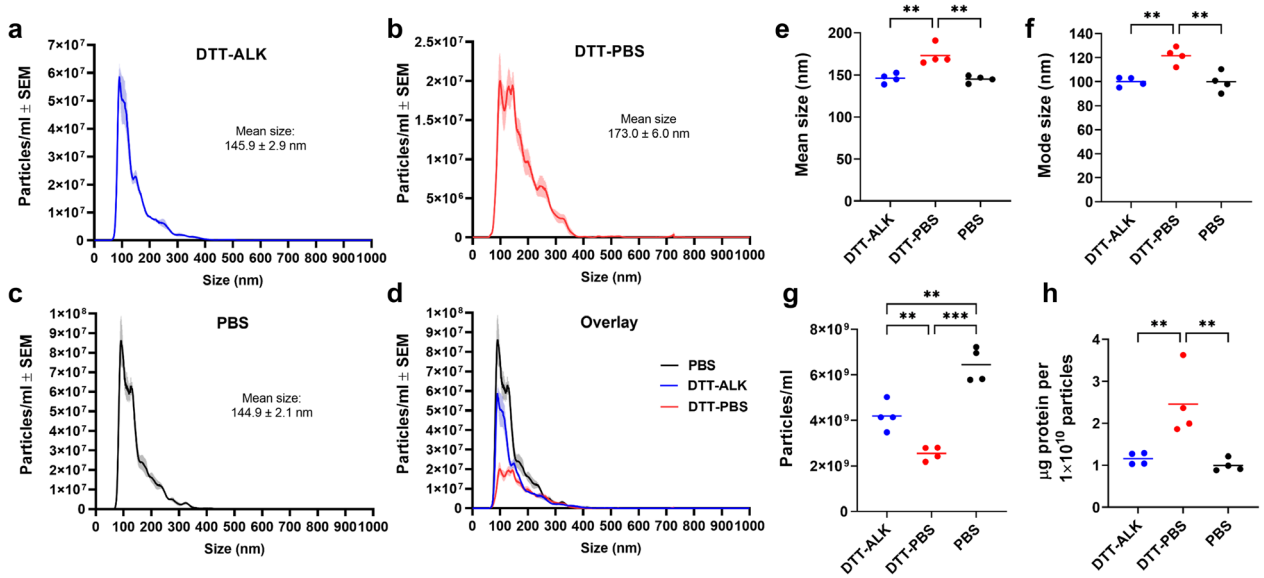

FIGURE 2 NanoSight nanoparticle tracking analysis of EVs isolated from EPS-urine. **a-d,** Size distributions of particles isolated via (a) DTT-ALK, (b) DTT-PBS, (c) PBS methods, or their composite overlay (d). The *y*-axis represents the total number of particles in the resuspended P4 fraction divided by the volume of EPS-urine used for EV-enrichment. Plotted lines represent the average number of particles/ml based upon four experimental replicates and shading represents the standard error. The mean particle size ± standard error of the mean is shown for each condition. **e-h,** Scatter plots from four experiments that compare the mean particle size (e), mode particle size (f), total particles (g), and total protein per particle (h). Each point represents an average value of 5 technical replicates, and the bar represents the mean of four experimental replicates. Ordinary one-way ANOVA and Tukey *post hoc* analyses were performed. Tukey adjusted *p*-value is shown [*** (<0.001), ** (0.001 to 0.01)].

with significantly lower mean and mode particle sizes when compared to DTT-PBS (Figure 2e,f). Interestingly, the DTT-PBS method had the lowest overall average particle yield per mL of EPS-urine ($2.5 \times 10^9 \pm 3.0 \times 10^8$ SD), when compared to the PBS ($6.4 \times 10^9 \pm 7.5 \times 10^8$ SD) or DTT-ALK ($4.2 \times 10^9 \pm 6.3 \times 10^8$ SD) methods (Figure 2 g). Although the highest particle yield was observed for the PBS method, this may be the result of THP polymers/aggregates confounding particle enumeration. We combined NTA and protein assay results to estimate protein/particle ratio (μg of protein per 1×10^{10} particles). The DTT-PBS EV pellet had a significantly higher average protein/particle ratio (2.46 ± 0.80 SD) than the other methods (DTT-ALK 1.16 ± 0.14 SD; PBS 1.00 ± 0.15 SD), suggesting this method had the lowest purity (Figure 2h) (Webber & Clayton, 2013). Collectively, these findings demonstrate that the DTT-ALK approach yielded uEVs with optimal efficiency, structural integrity, and reduced urine THP contaminants.

3.2 | Relative portion of total urine EVs trapped in THP matrix

Although it has been demonstrated that depolymerization of the THP matrix in the low-speed pellet can release THP-entrapped EVs (Fernández-Llama et al., 2010), it is unclear what proportion of total uEVs are sequestered within the THP matrix versus free-floating in urine. Therefore, we directly enumerated the impact of DTT-mediated uEV recovery on uEV yield in a separate experiment. Supernatant from the initial low-speed (20,000 g) spin of EPS-urine (SN1) and supernatant from the repeated low-speed spin of the DTT-treated 20,000 g pellet (SN2) were processed in parallel, and crude EV pellets were both filtered and washed with the alkaline solution (Figure 3a). NTA analysis revealed that the implementation of DTT depolymerization recovered small vesicles from the 20,000 g pellet whose size distribution overlapped with the SN1-derived uEVs (Figure 3b-d). Additionally, the particle yield from the matrix-bound SN2-derived uEVs had approximately 5 fold fewer total particles than the SN1-derived uEVs (SN1-derived = 3.3×10^9, SN2-derived = 6.6×10^8), indicating that the reduction of THP network by DTT treatment of the low-speed pellet resulted in a uEV yield increase of approximately 20% (Figure 3e).

3.3 | Comparative proteomic analysis of uEVs

To reveal the global protein composition of uEVs, we conducted in-depth proteomic analysis of uEVs isolated by the DTT-ALK, DTT-PBS, and PBS methodologies. Label-free quantitative LC-MS/MS of the uEV P4 fractions was performed. As shown in Figure 4a, the greatest average number of identified unique protein groups was found in uEVs enriched with the DTT-ALK

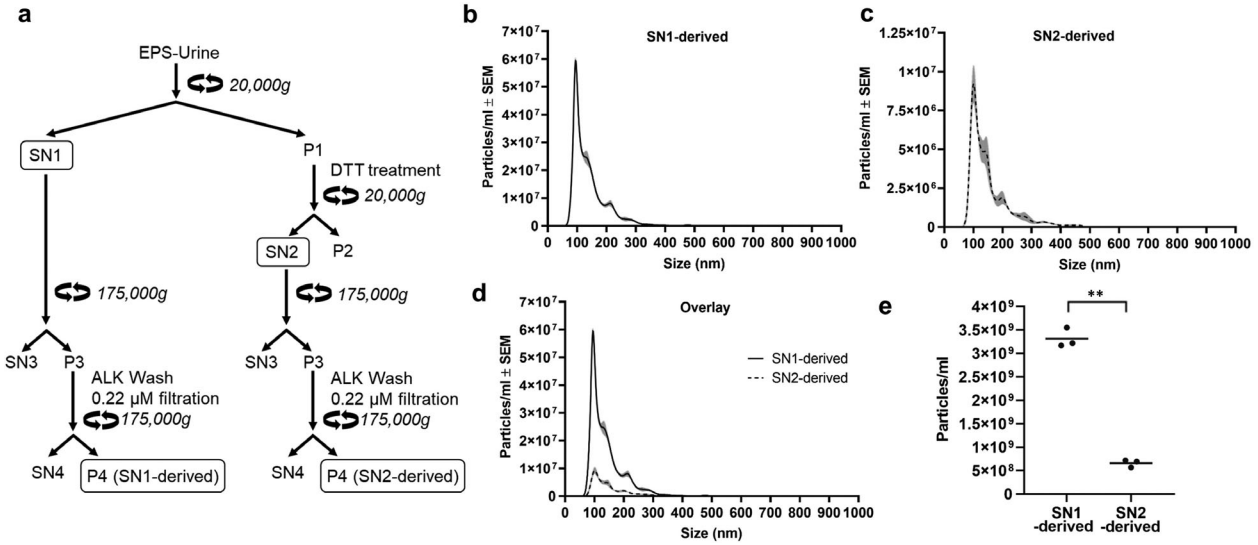

FIGURE 3 NanoSight nanoparticle tracking analysis of EPS-urine EVs derived from SN1 and SN2. **a,** EV isolation was performed as described in Figure 1, except the cell-free EPS-urine fraction (SN1) and the supernatant containing EVs released from the THP matrix after DTT treatment (SN2) were not combined before 175,000 g ultracentrifugation. **b-d,** Size distributions of particles in SN1-derived P4 (b), SN2-derived P4 (c), and their overlay (d). The *y*-axis represents the total number of particles in resuspended P4 divided by the volume of EPS-urine used for EV-enrichment. Plotted lines represent the average number of particles/mL based upon three experimental replicates, and shading represents the standard error. **e,** Particle concentration (particles per ml of EPS-urine) of SN1-derived P4 and SN2-derived P4. Each point represents an experimental replicate and is the average of 5 technical replicates. The bar represents the mean of the three experimental replicates for each condition (SN1-derived = 3.3×10^9, SN2-derived = 6.6×10^8). Paired *t*-test ** ($p = 0.001$).

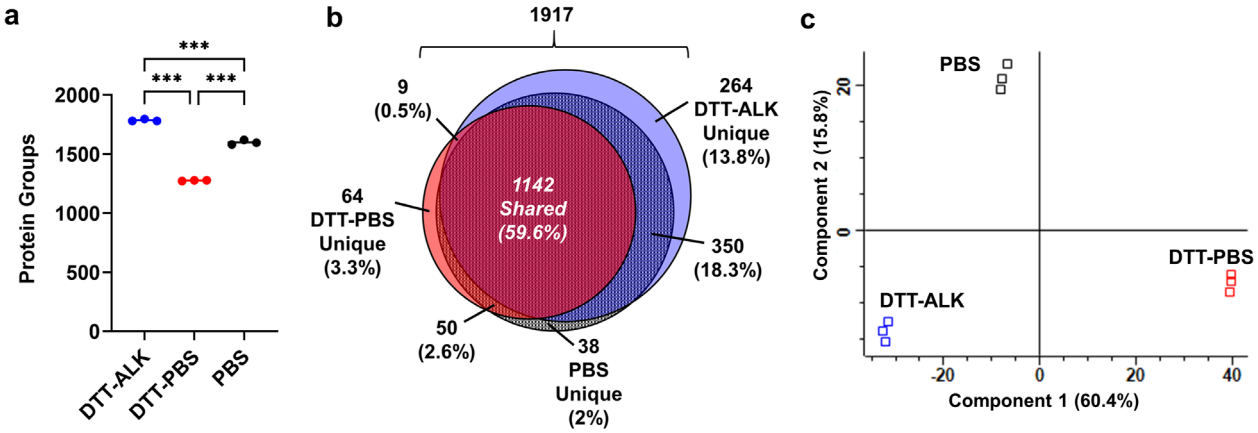

FIGURE 4 Comparison of protein groups identified by LC-MS/MS for each EV isolation approach. **a,** Scatter plot of total number of protein groups identified. Each point represents a technical replicate. Bar indicates mean. A one-way ANOVA with Tukey *post hoc* analyses was performed. Tukey adjusted *p*-value is shown (***$p < 0.001$). **b,** Area proportional Venn diagram of protein groups that were identified using strict selection criteria. Annotated are the number and proportional distribution of unique identities for all EV isolation approaches. **c,** Principal component analysis of LFQ intensities of the 1917 protein groups after $\log_2$ transformation and imputation of missing values.

approach (1786 ± 9.8 SD), followed by the PBS (1598 ± 19.7 SD) and DTT-PBS (1275 ± 2.9 SD) approaches. We then restricted the analysis to protein groups that were observed in at least 2/3 LC-MS/MS technical replicates of at least one condition. A Venn diagram of the remaining 1917 protein groups meeting this criterion (Supplementary Table S2) is shown in Figure 4b. Of these protein groups, the DTT-ALK method yielded 1765 unique protein groups, the DTT-PBS method yielded 1265 unique protein groups and the PBS method yielded 1580 unique protein groups. A total of 60% (1142) of the total protein groups were common to all conditions. Principal component analysis demonstrated that EVs isolated by the DTT-ALK condition were more similar to the PBS (rather than DTT-PBS) condition (Figure 4c). Spearman correlation analysis based upon scatter plots of $\log_2$ transformed LFQ intensities confirmed the high similarity of technical replicates within each method ($r \geq 0.99$). Interestingly, a relatively closer correlation of protein intensity for DTT-ALK and PBS (average $r = 0.957$) compared to DTT-PBS (average $r = 0.817$) was observed (Supplementary Figure S2). These results underscore the differential protein content of each uEV preparation and indicate that uEVs isolated by DTT-ALK and PBS exhibited a relatively greater degree of similarity.

3.4 | Differential enrichment of biologically-relevant proteins from isolated uEV preparations

To identify protein groups with a difference in mean $\log_2$(LFQ intensity) between the three conditions, we performed a one-way ANOVA (s0 = 2, FDR < 0.05) using the Perseus software platform (Tyanova & Cox, 2018). The resulting 1182 protein groups were subjected to hierarchical clustering to generate an intensity heatmap. The four largest clusters with different patterns in protein intensity across conditions (containing 191, 149, 115, and 627 protein groups) were chosen for further analysis (Figure 5a). Among these, the clusters of 191 and 149 protein groups displayed a relative intensity pattern of lower intensity in DTT-ALK compared to DTT-PBS, and the clusters of 115 and 627 protein groups had higher intensity in DTT-ALK compared to DTT-PBS (Figure 5b). As a reference, THP was identified among the cluster of 149 protein groups.

We next characterized the uEV preparations by examination of the subcellular location annotations of proteins identified in the four clusters. Gene ontology (GO) cellular component enrichment analysis was conducted to develop a global enrichment map, and we overlaid the map with the corresponding intensity pattern clusters (Figure 5c). GO terms related to secretory granules were enriched within all clusters. Proteins significantly enriched within the EVs isolated with the DTT-PBS method (cluster 191 and 149) were dominated by extracellular matrix (ECM) and secreted blood proteins. In contrast, proteins enriched in EVs isolated using the DTT-ALK method (cluster 627 and 115) were associated with cellular organelles involved in EV biogenesis including endosome, coated vesicles, cell junction, proteasome, and cytoskeleton. Consistent with these results, GO analysis for the biological function of each cluster revealed that terms related to ECM organization, GAGs metabolism, proteolysis, blood coagulation, platelet degranulation, lipoprotein remodelling, and humoral immune response were enriched in EVs prepared with the DTT-PBS approach. Conversely, vesicle-mediated transport, membrane docking, Rab/Ras signalling, autophagy, RNA and protein translocation, nucleic acid and protein metabolism, and antigen processing and presentation were enriched in EVs isolated with the DTT-ALK method (Supplementary Figure S3). The over-representation of these GO terms is consistent with the components and functions of EVs (Kowal et al., 2014).

3.5 | Differential depletion of selected urinary proteins and putative EV contaminants

To evaluate the relative purity of the uEV preparations, we examined the full data set (1917 protein groups) for the relative enrichment of a manually-curated list of 32 high-abundance urine proteins (THP, albumin, alpha-1-antitrypsin, haemoglobins, apolipoproteins, coagulants, complements, alpha and beta-globulins, and immunoglobulins). Many of these proteins were considered in MISEV2018 to be part of "major components of non-EV co-isolated structures" (Théry et al., 2018). As shown in the heatmap (Figure 6a), these proteins displayed higher intensity levels in EVs isolated with DTT-PBS and PBS methods compared to the DTT-ALK method. The LFQ intensities of the two most abundant proteins in urine (THP and albumin) were specifically compared. Consistent with western blot analysis (Figure 1c), the mean intensity of THP was lowest within the DTT-ALK condition (2.64×10^9) as compared to DTT-PBS (9.54×10^{10}) and PBS (1.57×10^{11}), representing a 36-fold and 60-fold reduction, respectively (Figure 6b). Although serum albumin is routinely filtered out as a potential contaminant by the Perseus software and not included as part of the 1917 protein groups (Supplementary Table S2), we also examined its intensity distribution (Figure 6c). Serum albumin had the lowest mean intensity in the DTT-ALK condition (3.07×10^9), which was 15-fold lower than in DTT-PBS (4.72×10^{10}) and 2-fold lower than in PBS (6.02×10^9). Similarly, the average intensity across the remaining 30 plasma-filtered proteins was also lowest in the DTT-ALK condition (9.87×10^7), which was 7-fold lower than in DTT-PBS (7.24×10^8) and 2.5-fold lower than in PBS (2.48×10^8) (Figure 6d).

Next, we compared our data with a recently published list of 684 putative contaminants of urinary vesicles (Dhondt et al., 2020). This list was based upon LC-MS/MS analysis of urinary EVs isolated by density gradient ultracentrifugation. We observed 81 of these putative contaminating proteins in our data, five of which were in our list of 32 high-abundance proteins (i.e., C4A, C4B, CFI, HP, IGHM). A total of 79 of the 81 proteins were present in the DTT-PBS condition, while 34 and 47 proteins were in the DTT-ALK and PBS conditions, respectively. Quantitation of the average intensity across these 81 proteins revealed a significantly higher mean intensity level in the DTT-PBS (5.65×10^7) and PBS (2.62×10^7) conditions compared to the DTT-ALK condition (1.75×10^7) (Figure 6e).

Given the known presence of extracellular matrix (ECM) molecules on the surface of EVs (Buzás et al., 2018; Théry et al., 2018), we investigated the relative intensity of ECM proteins for each of the three isolation methods. Identified ECM molecules included collagens (COL18A1, COL15A1, COL4A2, COL6A1), heparan sulfate proteoglycans (AGRN, HSPG2), chondroitin sulfate proteoglycans (CSPG4), small leucine-rich proteoglycans (BGN, LUM), as well as bridge components (FN1, LAMA5/B2/C1, NID1, VTN, LGALS3BP), and fibulins (EFEMP1, FBLN2, HMCN1). The intensity of the selected ECM proteins was significantly reduced in uEVs isolated via the DTT-ALK approach (Figure 6f). Isolation of uEVs with the DTT-ALK approach resulted in reduced intensity of fibronectin (FN1), a well-studied ECM protein reported to interact with EVs (Buzás et al., 2018), by 19-fold (DTT-PBS) and 3-fold (PBS) (Figure 6g). Quantitation of the remaining ECM proteins revealed a similar intensity profile across the three methods (Figure 6h), demonstrating the efficiency of the DTT-ALK method to release non-covalently attached surface proteins from EVs.

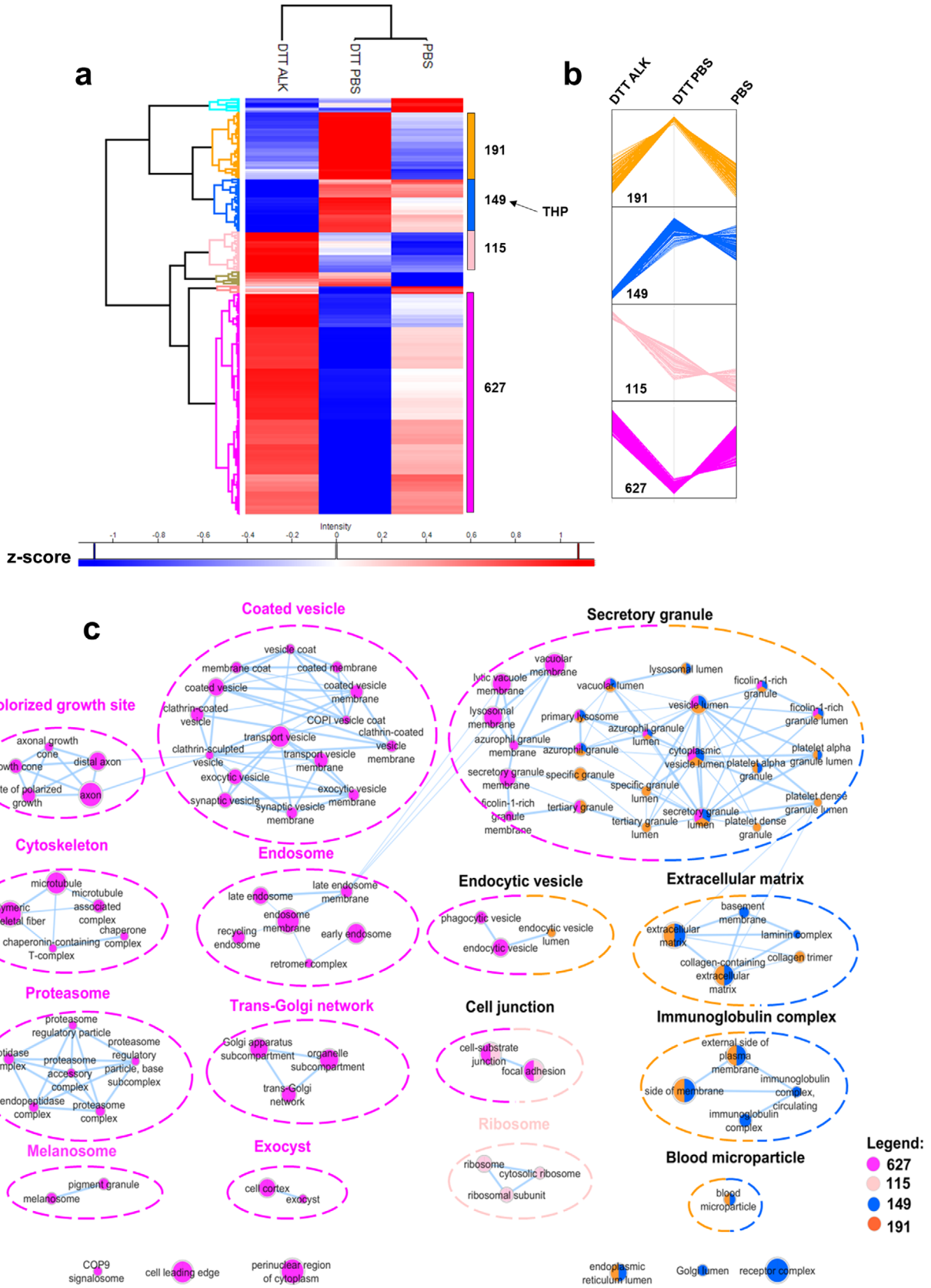

FIGURE 5 Characterization of differentially enriched proteins in uEVs. **a,** Heatmap with hierarchical clustering of 1182 protein groups found to be differentially abundant following ANOVA analysis (s0 = 2, FDR < 0.05). LFQ intensities were $\log_2$ transformed and missing values were imputed (as described in the methods section) before ANOVA. Three LC-MS/MS technical replicates $\log_2$(LFQ intensities) were averaged, and averages were *z*-score normalized for heatmap generation. Red and blue indicate high and low *z*-scores as indicated in the bar graph. The four major clusters are highlighted, and the number of

3.6 | Relative enrichment of EV markers and membrane-associated proteins

We further mined the proteomic data to determine the relative intensity of proteins involved in EV biogenesis within our dataset: membrane proteins (tetraspanins, LAMP1/2), cytosolic proteins (heat shock proteins, annexins, lipid raft proteins FLOT1/2), ESCRT components, and proteins responsible for vesicle transport or membrane fusion such as Rab and SNARE family members (Supplementary Figure S4) (Hessvik & Llorente, 2018; Kowal et al., 2014). Notably, we identified all of the subunits of the four ESCRT complexes (ESCRT-0 through ESCRT-III) in uEVs. A total of 53 (93%) EV markers were observed in all conditions, and a total of 48 (84%) of them were present in the 3rd and 4th quartile of the scaled intensity ranking (highest 75%–100%) of each proteome (Supplementary Figure S4). ANOVA analysis ($s0 = 2$, FDR < 0.05) of all 57 markers revealed 26 proteins with a significant difference in mean LFQ intensity between enrichment approaches. When visualizing the intensity of these 26 proteins, we observed a clear trend that EVs isolated by the DTT-ALK had the highest relative intensity of EV markers while EVs prepared by DTT-PBS had the lowest intensity levels (Figure 7a-b).

Since sodium carbonate can separate integral membrane proteins (IMPs) from peripheral membrane protein (PMPs) (Fujiki, Fowler, et al., 1982; Fujiki, Hubbard, et al., 1982), we explored the impact of the three EV enrichment strategies on the content of different classes of membrane-associated proteins. By cross-referencing the annotations from UniProtKB, we categorized membrane-associated proteins into six types: outer leaflet peripheral membrane proteins (OLPMPs), GPI-anchored proteins, single-pass IMPs, multi-pass IMPs, lipid-anchored proteins, and inner leaflet peripheral membrane proteins (ILPMPs) (Figure 7c). We supplemented the UniprotKB annotations for ILPMPs with the search terms cytoplasmic side, cytoplasm, and cell junction. For OLPMPs, the terms secreted, cell surface, and endocytosis were included. In total, 675 of 1917 evaluable EV proteins (35%) were classified as membrane-associated proteins (Supplementary Table S3), which is in line with a recent analysis of membrane proteins from proteomic data in Exocarta (40%) and Vesiclepedia (21%) databases (Kalra et al., 2012; Keerthikumar et al., 2016). We observed that the relative intensity of OLPMPs was significantly reduced in DTT-ALK isolated uEVs when compared to either PBS or DTT-PBS (Figure 7d-e). Isolation of uEVs with the DTT-ALK method also enhanced the relative intensity of multi-pass IMP, lipid-anchored membrane proteins, and ILPMPs. The relative enrichment of IMPs and ILPMPs and reduction of OLPMPs is consistent with the DTT-ALK approach yielding uEVs of greater purity.

3.7 | Relative enrichment of prostate cancer-associated and tissue-specific proteins

We examined the relative enrichment of prostate-specific and prostate cancer-associated biomarkers between methodologies and assembled a list of 27 PCa biomarker proteins present in our dataset that have been verified as present in uEVs from the literature (Dhondt et al., 2020; Drake & Kislinger, 2014; Gonzales et al., 2009; Øverbye et al., 2015; Wang et al., 2012). In addition, we searched our dataset against the TiGER (Tissue-specific Gene Expression and Regulation) database for gene transcripts "preferentially expressed in prostate" that were filtered for evidence of protein expression in the Human Protein Atlas (HPA) and evidence of association with PCa (X. Liu et al., 2008; Uhlén et al., 2015). The resulting list consisted of 33 putative PCa biomarkers. By ANOVA ($s0 = 2$, FDR < 0.05), we observed a significant difference in average intensity across the three methods for 27/33 proteins (Figure 8a). Secreted proteins including prostate acid phosphate (ACPP/PAP), kallikrein-2 (KLK2), and prostate-specific antigen (KLK3/PSA), were reduced in uEVs isolated by DTT-ALK and enriched in uEVs prepared by DTT-PBS. In contrast, transmembrane protein biomarkers including metalloreductase 2/4 (STEAP2/4), anoctamin 7 (ANO7), glutamate carboxypeptidase 2 (FOLH1/PSMA), retinol dehydrogenase 11 (RDH11), dipeptidyl peptidase 4 (DPP4), and intracellular proteins such as peptidyl-prolyl cis-trans isomerase FKBP5 (FKBP5), fatty acid synthase (FASN), sorbitol dehydrogenase (SORD), protein NDRG1 (NDRG1), copine-4 (CPNE4) were significantly enriched by the DTT-ALK approach. These results support the idea that the DTT-ALK approach enriches for uEVs that derive from the prostate.

We next employed Ingenuity Pathway Analysis (IPA) to identify canonical PCa-associated signalling pathways in uEVs prepared by all three methods. A total of 26 PCa-associated signalling molecules were identified in our data, and 19 were shared by all conditions (Figure 8b, Supplementary Figure S5). The remaining seven of the 26 signalling proteins (PIK3R1, AKT1, mTOR, PDPK1, RELA, MAPK3, PA2G4) involved in PI3K-AKT-mTOR, NF-κB, Ras-Raf-MEK-ERK, and Rb-E2F1 pathways were observed in uEVs isolated by the DTT-ALK approach. Similarly, 5/7 proteins were uniquely observed in the DTT-ALK method, while only two (AKT1 and PIK3R1) were identified in the PBS condition; none were identified with the DTT-PBS

protein groups per cluster is indicated (191, 149, 115, and 627). **b,** Profile plots of four colour-coded clusters showing trends in protein group intensity across conditions. Cluster 191 - orange, cluster 149 - blue, cluster 115 - light pink, cluster 627 - magenta. **c,** Network map of cellular components enriched within the four heatmap cluster protein groups. Nodes represent enriched GO terms with colour reflecting the clusters and the size corresponding to the number of proteins in that set. Edges represent GO defined relations, and line thickness correlates to the degree of overlap between nodes. Gene-sets that did not pass the enrichment significance threshold are not shown. Groups of functionally related gene-sets were manually circled by a dotted line and assigned a label which both are colour-matched with the clusters while the shared pathways are shown by black headers.

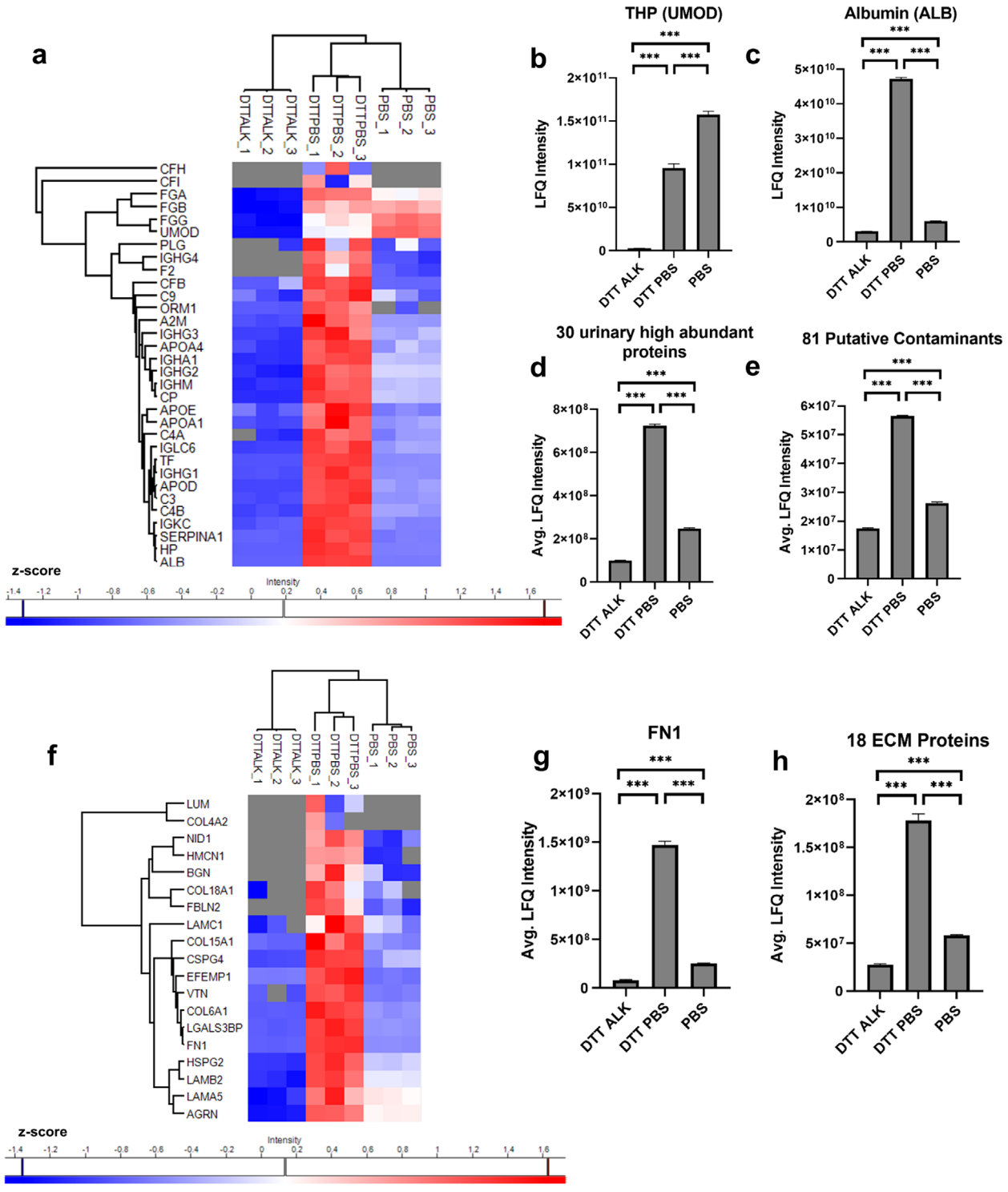

FIGURE 6 Relative depletion of high-abundance urine proteins, putative contaminants, and selected ECM proteins associated with uEVs. **a,** Heatmap with hierarchical clustering of z-score normalized LFQ intensities of 32 high-abundance urine proteins: THP (UMOD), serum albumin (ALB), and 30 proteins derived from plasma [apolipoproteins (APOA1, APOA4, APOD, APOE), coagulants (F2, FGA, FGB, FGG), complements (C3, C4A, C4B, C9, CFB, CFH, CFI), α1 Globulins (SERP1NA1, ORM1), α2 Globulins (A2M, CP, HP), β Globulins (PLG, TF), and immunoglobulins (IGHA1, IGHG1, IGHG2, IGHG3, IGHG4, IGHM, IGKC, IGLC6)]. Red and blue colors correlate with high and low z-scores. Missing values are in grey. Technical replicates for each method are denoted as 1, 2, or 3. **b-e,** Bar graphs of LFQ intensity (mean ± SD) of (b) THP, (c) albumin, (d) 30 urinary proteins derived from plasma, and (e) 81 putative contaminants of uEVs. **f,** Heatmap with hierarchical clustering of *z*-score normalized LFQ intensities of 19 selected ECM proteins. Red and blue indicate high and low *z*-scores as indicated in the bar graph. Missing values are in grey. Technical replicates for each method are denoted as 1, 2, or 3. **g-h,** Bar graphs of LFQ intensity (mean ± SD) of (g) fibronectin and (h) 18 remaining ECM proteins. Ordinary one-way ANOVA and Tukey *post hoc* analyses were performed. Tukey adjusted *p*-value is shown (***$p < 0.001$).

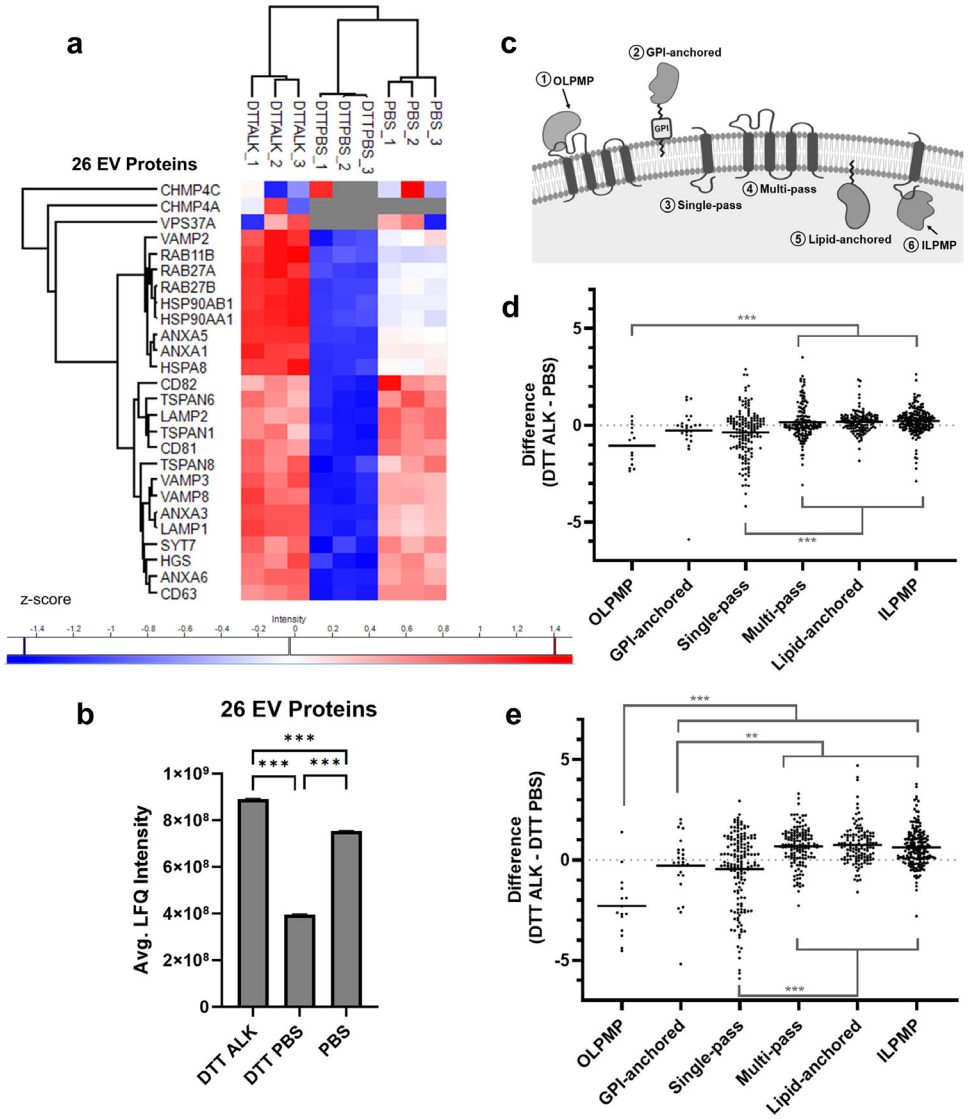

FIGURE 7 Relative enrichment of putative EV marker proteins and classes of membrane proteins in uEVs. **a,** Heatmap of z-score normalized LFQ intensities of 26 EV marker proteins. Red and blue indicate high and low *z*-scores as indicated in the bar graph. Missing values are in gray. Technical replicates for each methodology are denoted as 1, 2, or 3. **b,** Bar graph of average LFQ intensity (mean ± SD) of 26 EV marker proteins shown in **a**. Ordinary one-way ANOVA and Tukey *post hoc* analyses were performed. Tukey adjusted *p*-value is shown (***$p < 0.001$). **c,** Diagram (created with Biorender.com) showing the surface orientation of six membrane protein types: outer-leaflet peripheral membrane protein (OLPMP), GPI-anchored, single-pass transmembrane, multi-pass transmembrane, lipid-anchored, and inner-leaflet peripheral membrane protein (ILPMP). The cytosol is coloured grey. **d-e,** Dot plot of the difference between average $\log_2$ transformed LFQ intensity (with missing values imputed) of proteins enriched in (d) DTT-ALK versus PBS and (e) DTT-ALK versus DTT-PBS methodology. The bar indicates the mean. Dotted grey line represents no fold change ($y = 0$). Ordinary one-way ANOVA with Tukey *post hoc* analyses were performed. Tukey adjusted *p*-value is shown [*** (<0.001), ** (0.001 to 0.01)].

approach. Interestingly, these seven proteins were all present in the 1st and 2nd quartiles (the lowest 25%–50%) of the scaled intensity ranking of DTT-ALK proteome, suggesting DTT-ALK approach allows deeper uEV proteome coverage (Figure 8b, Supplementary Figure S5c). In addition, many other signalling molecules involved in other PCa-associated pathways such as AR, RAS, catenin β, and GSTP-1 signalling had higher intensity levels in uEVs prepared by DTT-ALK compared to DTT-PBS. Similar results were observed when comparing the DTT-ALK to PBS method. These results suggest that isolation of uEVs with the DTT-ALK approach enriches for prostate-derived and PCa-associated proteins.

We also assessed the level of enrichment of other tissue-specific proteins in our data. We performed functional enrichment analysis (g:Profiler against HPA database) of DTT-ALK uEV proteins and found that "kidney," "prostate," and "seminal vesicle" were the most significantly enriched terms. A similar analysis was conducted on the available datasets of two recently published studies that employed dUC or density gradient UC for isolation of uEVs (Dhondt et al., 2020; Fujita et al., 2017). "Kidney" was the top term across all datasets, and the top five terms in our dataset were in line with the previous reports (Supplementary Figure S6a). In addition, we looked for the presence of several well-known markers of different regions of the urogenital tract

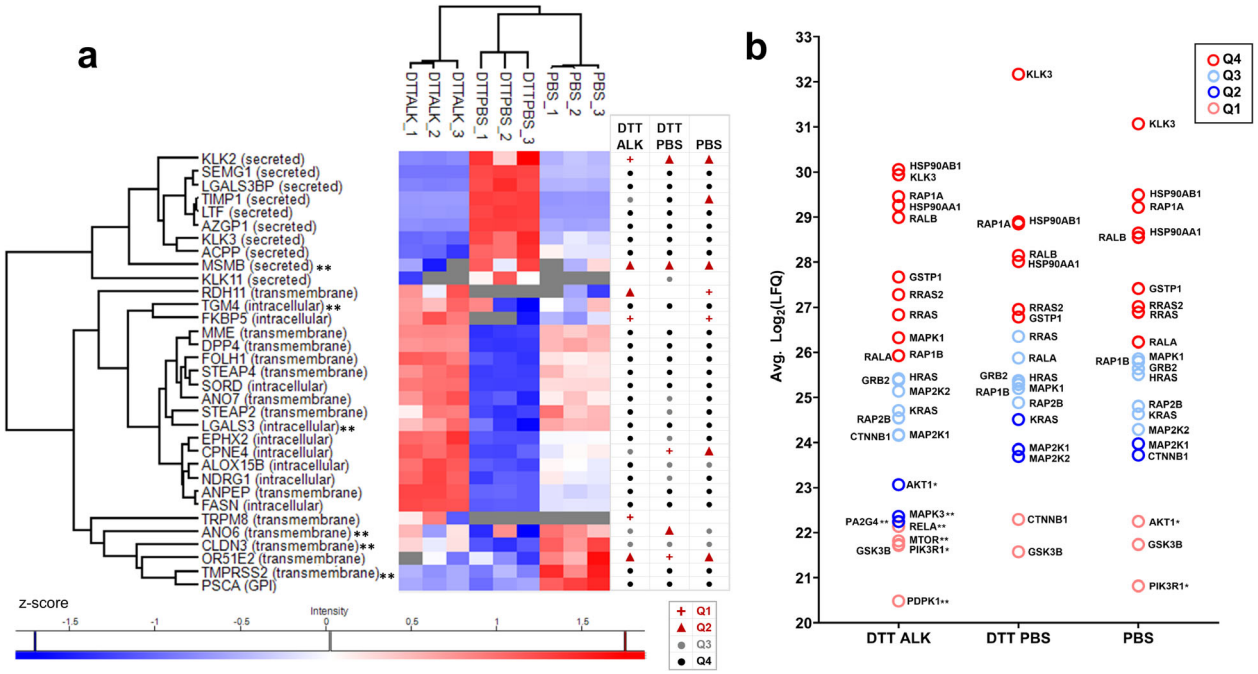

FIGURE 8 Relative enrichment of prostate-specific and prostate cancer associated proteins in uEVs. **a,** Heatmap of *z*-score normalized LFQ intensities of 33 selected proteins. Red and blue indicate high and low *z*-scores as indicated in the bar graph. Missing values are in grey. Technical replicates for each methodology are denoted as 1, 2, or 3. Gene name of the protein groups is shown with cellular localization noted in parenthesis. A total of 27/33 were significant by ANOVA (s0 = 2, FDR < 0.05). ** denotes non-significance. The quartile ranking of each protein (based upon average $\log_2$(LFQ intensity) is marked with a symbol as shown in the legend. **b,** Stacked scatter plot depicting the average $\log_2$(LFQ intensities) of 26 PCa signalling molecules in each condition. Colour code indicates quartile (as shown in the legend). 19 proteins were identified in all conditions. **Denotes the five proteins exclusively detected in DTT-ALK. * Denotes the two proteins detected in DTT-ALK and PBS but not DTT-PBS.

among the proteins identified in uEVs enriched by the DTT-ALK, DTT-PBS, and/or PBS methods (Supplementary Figure S6b). The post-DRE uEVs preparations contained proteins derived from renal epithelial cells from a variety of locations in the kidney (glomerulus, proximal tubule, thick ascending limb of Henle, distal convoluted tubule, and the collecting duct), transitional epithelium of the urinary bladder, columnar epithelium of seminal vesicles, and prostate—supporting the notion that urine EVs originate from all regions of the urogenital tract. These tissue-specific proteins were distributed across all quartiles of ranked protein intensity, and the DTT-ALK method enabled identification of several of the lower intensity proteins (UPK1B, SLC22A8, and SLC5A2) that were not detected in the DTT-PBS and/or PBS condition (Supplementary Figure S6d-e). Collectively, these results demonstrate that the isolation of uEVs by the DTT-ALK approach improved sampling of prostate biology in post DRE-urine.

4 | DISCUSSION

Protein contaminants can be co-isolated with EVs during EV-enrichment, and improving EV purity is a desirable goal when using highly sensitive downstream methods such as proteomics. A vast array of proteins have been reported to interact with the EV surface to form a "protein corona" (Buzás et al., 2018; Palviainen et al., 2020). Although some of these proteins may be isolation artifacts, accumulating evidence suggests that protein corona on EVs are stable, highly diverse, and heterogeneous and include abundant blood proteins such as fibrinogen, gamma globulin, complement, and serum albumin (Karasu et al., 2018; Palviainen et al., 2020). Multiple intermolecular forces (ionic interactions, hydrophobic interactions, hydrogen bonding, and van der Waals forces), as well as protein conformation between corona proteins and EVs, are likely responsible for these noncovalent interaction with variable affinities. While protein corona may add extra attributes to EVs, they can mask or even modulate the topology of source-specific structural EV molecules, resulting in biased isolation and analysis as well as skewed functional annotation of EVs. However, the removal of protein corona from EVs is difficult. Previous methods employing enzymes such as trypsin or protease K may digest some degree of protein corona, but structural EV proteins can also be destroyed (Choi et al., 2020; Cvjetkovic et al., 2016; R. Xu, et al., 2019). Here through adjusting the pH value of buffer at the last step of EVs isolation, our study provides an effective way to reduce circulating contaminants and constituents of protein corona.

At least a portion of these corona proteins is attached to EVs via specific molecular recognition. For instance, it has been reported that fibronectin (FN1) can be attached to EV surface through the binding of membranous partner proteins such as integrins and heparin sulfate proteoglycans (Purushothaman et al., 2016; Rieu et al., 2000). Lactadherin (MFGE8) and growth-arrest specific protein 6 (Gas6) were reported to interact with EVs through binding to externalized phosphatidylserine (PS), a characteristic feature of many EVs (Buzás et al., 2018; Véron et al., 2005). In addition, current methods do not discriminate whether the deposition of protein corona on EVs is a post EV secretion event or realized during EV biogenesis. It is likely that most abundant blood and urine proteins are at least partly acquired after EVs are generated. However, recent studies showed that some components of protein corona such as fibronectin, complement C3, and cytokine TGF-β can be endocytosed by cells and then targeted to MVBs, and subsequently re-secreted on the exofacial surface of EVs (Buzás et al., 2018; Ko & Naora, 2020; Sung et al., 2015). EV surface VEGFs can stimulate tumour angiogenesis and enable tumours to evade anti-angiogenic therapy (Ko & Naora, 2020). EV fibronectin was found to promote adhesion formation and directional cancer cell motility (Sung et al., 2015). Protein corona of EVs can be utilized to alter the biodistribution, stability, and target specificity of EVs as drug delivery vehicles (Hu et al., 2020; Murphy et al., 2019). Clarification of the mechanisms of biogeneration and divergence of protein corona is needed to understand the impact of an alkaline wash step on the recovery of biologically active/relevant EVs.

In contrast to previous reports, we found that the integrity of the EV membrane was not affected by sodium carbonate treatment under standard dUC-based EVs isolation conditions (Fujiki, Fowler, et al., 1982; Fujiki, Hubbard, et al., 1982). Fujiki et al. reported that a high pH buffer could convert closed microsome vesicles to an open membrane sheet and distinguish integral membrane proteins (IMPs) from peripheral membrane proteins (PMPs) (Fujiki, Fowler, et al., 1982; Fujiki, Hubbard, et al., 1982). Largely as a result of this finding, sodium carbonate has been deemed as a canonical method to remove PMPs from intracellular/organelle membrane fractions (Kaiser et al., 2009; H. Kim et al., 2015; Ruan et al., 2008; Zhu et al., 2005). In fact, several groups employed sodium carbonate to fractionate the EV membrane and determine the location of EV proteins presuming that this method impacts EV structure similarly to microsome structure (Campanella et al., 2012; Emmanouilidou et al., 2010; Jang et al., 2019; Jeppesen et al., 2014; Palmisano et al., 2012; X. Xu, et al., 2019). We report that incorporation of a carbonate wash into dUC workflow does not disrupt the EV membrane, but can remove external PMPs from EVs. We demonstrated this through the observation of intact vesicles under TEM and by efficient identification of luminal proteins in our uEV proteome. We also observed that only outer leaflet PMPs, reversibly attached to the EV membrane, were significantly depleted by carbonate treatment. Other covalently-attached or embedded types including GPI-linked, multi-pass IMPs, single-pass IMPs, and lipid-anchored were retained. In addition, non-covalently attached inner leaflet PMPs were not affected, strongly supporting the integrity of EV membrane. In line with our findings, a prior study demonstrated that the integrity of uEVs was not harmed by alkaline buffer (Puhka et al., 2017). We additionally tested different carbonate treatment conditions and found that only extended incubation at higher temperature or with additional physical shearing disrupted EV structure (data not shown). Since microsomes are vesicle-like artifacts re-formed from broken pieces of hepatocyte endoplasmic reticulum, peroxisome, or mitochondrion during tissue homogenization, such vesicles may have defective membrane structure fragile to the harsh conditions (Fujiki, Fowler, et al., 1982; Fujiki, Hubbard, et al., 1982). The well-organized membrane structure together with other physical characteristics of EVs (large surface to volume ratio, shape, size, and curvature) likely confers EVs resistance to physico-chemical changes in their environment. Our findings underscore the value of the new approach to effectively isolate structurally intact EVs, as well as the potential to discriminate external PMPs from other EV membrane-associated proteins.

Since THP is the most common urine protein and polymerizes to form extensive lattice-like networks in urine, it represents a significant bottleneck to successful isolation and protein profiling of uEVs. A number of strategies have been attempted to eliminate THP contamination with limited success (Chen et al., 2020; Kosanović & Janković, 2014; Z. Liu et al., 2018; Musante et al., 2012; Øverbye et al., 2015; X. Xu, et al., 2019). For example, the addition of $ZnSO_4$ to urine is only effective with fresh urine, relegating valuable urine biobanks inaccessible to study (Z. Liu et al., 2018). Prior to these studies, the resuspension of low-speed pellet with reducing agent DTT or the dilution of urine with an alkaline buffer with low ionic strength was reported to disrupt or loosen the THP polymeric meshwork effectively, presumably releasing the trapped uEVs and increasing EV yield (Fernández-Llama et al., 2010; Pisitkun et al., 2004; Puhka et al., 2017). However, uEVs isolated following these approaches were still contaminated with THP filaments and/or other high-abundance urinary proteins (Chen et al., 2020; Dhondt et al., 2020; Puhka et al., 2017; Santucci et al., 2019). In our current study, we compared the effect of DTT treatment of 20,000 g pellet on EV yield assessed by NanoSight. In agreement with the original report (Fernández-Llama et al., 2010), we found that DTT application to low-speed pellet releases the trapped uEVs and increases yield by approximately 20%.

THP matrix-bound uEVs and the interacting partner THP contain an array of glycans suggesting that THP-trapped EVs may have unique properties, destinations, and functions (Micanovic et al., 2020). We observed significant depletion of THP in the final uEV pellet only when both alkaline and DTT treatment were employed. Thus, the reduction of THP polymers by DTT treatment is a prerequisite for efficient alkaline wash. Conversely, we also observed that THP depolymerization shifted many constituents of protein corona to the high-speed uEV pellet, adding extra complexity to the EV proteome (Figure 6). This finding confirms that THP network traps many free proteins, as previously described (Musante et al., 2020; Rood et al., 2010; Wu et al., 2018), and also supports the notion that the formation of the protein corona is dynamic and extracellular milieu-dependent (Säemann et al., 2005; Simonsen & Münter, 2020). The addition of an alkaline wash step efficiently reversed the detrimental effect of DTT, depleting

THP as well as other contaminating proteins from the uEV pellet. In contrast, the PBS method does not employ DTT treatment and avoids such contamination to uEVs. These mechanisms could together explain the relative similarity in EV proteome of DTT-ALK to PBS rather than DTT-PBS. Our observation of a residual portion of THP associated with uEVs isolated via DTT-ALK suggests that GPI-anchored rather than secreted THP is a bona fide structural component of uEVs, although this warrants further investigation.

This study has several limitations. First, to develop the optimal method for uEV isolation from EPS-urine matrix, sample pooling was used as a strategy to compensate for high biological variation and limited volumes of individual samples. We are currently employing the new method on individual patient samples in a well-defined patient cohort of men with PCa to assess the intra- and inter-individual variability of uEVs in our efforts to develop novel biomarkers. Second, we focused our methodologic development toward small EVs in the 100 nm range and included a 0.22 μM filtration step to remove large EVs. The suitability of the DTT-ALK approach for large EVs and the impact of the filtration step on uEVs require further assessment. Third, unprocessed rather than cell-free EPS-urine was used for this study. Although we did not detect intracellular organelle proteins (calnexin, GM130, and cytochrome c), we cannot preclude their presence below the detection limits of Western blot and LC-MS/MS. Finally, in addition to depolymerization of the THP network, DTT may structurally impact EVs. Although our protocol depletes DTT through dilution and subsequent ultracentrifugation, the conclusions regarding the differential separation of EV corona proteins should be confirmed.

In summary, we developed an effective isolation method by integrating DTT treatment and alkaline wash into dUC for the isolation of uEVs with high purity and improved yield. The method represents an easily adopted and efficient dUC strategy for recovery of uEVs depleted of abundant urinary proteins as well as non-covalently bound protein corona constituents. The resulting preparation enables comprehensive deep profiling of prostate-derived uEVs by LC-MS/MS. Additionally, DTT treatment and alkaline wash can potentially be implemented in other uEV isolation workflows (reviewed in Erdbrügger et al., 2021; Liang et al., 2021), allowing for the assessment of THP-resident uEVs and further improvement in the purity of uEVs. These qualities may improve subsequent biomarker discovery and development from post-DRE urine clinical samples.

ACKNOWLEDGEMENTS

This work was supported by the National Cancer Institute's (NCI) Early Detection Research Network (EDRN) initiative under Grant U01CA214194. We thank Mary Ann Clements for the management of Eastern Virginia Medical School's Biorepository.

DECLARATION OF INTEREST STATEMENT

PCB sits on the Scientific Advisory Boards of Intersect Diagnostics Inc. and BioSymetrics Inc. The other authors report no conflicts of interest.

DISCLAIMERS

None.

DATA AVAILABILITY STATEMENT

We have submitted all relevant data of our experiments to the EV-TRACK knowledgebase (EV-TRACK ID: EV210199). The mass spectrometry proteomics data have been deposited to the ProteomeXchange Consortium via the PRIDE partner repository with the dataset identifier PXD026974.

PATIENT CONSENT

Samples were obtained from patients following informed consent and use of Institutional Review Board-approved protocols at Eastern Virginia Medical School and Urology of Virginia.

REFERENCES

Becker, A., Thakur, B. K., Weiss, J. M., Kim, H. S., Peinado, H., & Lyden, D. (2016). Extracellular vesicles in cancer: Cell-to-cell mediators of metastasis. *Cancer Cell*, *30*, 836–848. https://doi.org/10.1016/j.ccell.2016.10.009

Buzás, E. I., Tóth, E. Á., Sódar, B. W., & Szabó-Taylor, K. É. (2018). Molecular interactions at the surface of extracellular vesicles. *Semin Immunopathol*, *40*, 453–464. https://doi.org/10.1007/s00281-018-0682-0

Campanella, C., Bucchieri, F., Merendino, A. M., Fucarino, A., Burgio, G., Corona, D. F. V., Barbieri, G., David, S., Farina, F., Zummo, G., De Macario, E. C., Macario, A. J. L., & Cappello, F. (2012). The odyssey of Hsp60 from tumor cells to other destinations includes plasma membrane-associated stages and golgi and exosomal protein-trafficking modalities. *PLoS One*, *7*, e42008. https://doi.org/10.1371/journal.pone.0042008

Chen, Q. G., Chen, L., Zhong, Q. H., Zhang, L., Jiang, Y. H., Li, S. Q., Qin, T. Y., Sun, F., You, X. H., Yang, W. M., Huang, B., & Wang, X. Z. (2020). Optimization of urinary small extracellular vesicle isolation protocols: Implications in early diagnosis, stratification, treatment and prognosis of diseases in the era of personalized medicine. *American Journal of Translational Research*, *12*, 6302–6313. Available: http://www.ncbi.nlm.nih.gov/pubmed/33194031

Choi, D., Go, G., Kim, D. K., Lee, J., Park, S. M., Di Vizio, D., & Gho, Y. S. (2020). Quantitative proteomic analysis of trypsin-treated extracellular vesicles to identify the real-vesicular proteins. *Journal of Extracellular Vesicles*, *9*, 1757209. https://doi.org/10.1080/20013078.2020.1757209

Cox, J., & Mann, M. (2008). MaxQuant enables high peptide identification rates, individualized p.p.b.-range mass accuracies and proteome-wide protein quantification. *Nature Biotechnology*, *26*(12), 1367–1372. https://doi.org/10.1038/nbt.1511

Cox, J., Neuhauser, N., Michalski, A., Scheltema, R. A., Olsen, J. V., & Mann, M. (2011). Andromeda: A peptide search engine integrated into the MaxQuant environment. *Journal of Proteome Research*, *10*, 1794–1805. https://doi.org/10.1021/pr101065j

Cvjetkovic, A., Jang, S. C., Konečná, B., Höög, J. L., Sihlbom, C., Lässer, C., & Lötvall, J. (2016). Detailed analysis of protein topology of extracellular vesicles–evidence of unconventional membrane protein orientation. *Scientific Reports*, *6*, 36338. https://doi.org/10.1038/srep36338

Decramer, S., De Peredo, A. G., Breuil, B., Mischak, H., Monsarrat, B., Bascands, J.-L., & Schanstra, J. P. (2008). Urine in clinical proteomics. *Molecular & Cellular Proteomics*, *7*, 1850–1862. https://doi.org/10.1074/mcp.R800001-MCP200

Dhondt, B., Geeurickx, E., Tulkens, J., Van Deun, J., Vergauwen, G., Lippens, L., Miinalainen, I., Rappu, P., Heino, J., Ost, P., Lumen, N., De Wever, O., & Hendrix, A. (2020). Unravelling the proteomic landscape of extracellular vesicles in prostate cancer by density-based fractionation of urine. *Journal of Extracellular Vesicles*, *9*, 1736935. https://doi.org/10.1080/20013078.2020.1736935

Dhondt, B., Van Deun, J., Vermaerke, S., De Marco, A., Lumen, N., De Wever, O., & Hendrix, A. (2018). Urinary extracellular vesicle biomarkers in urological cancers: From discovery towards clinical implementation. *International Journal of Biochemistry & Cell Biology*, *99*, 236–256. https://doi.org/10.1016/j.biocel.2018.04.009

Drake, R. R., & Kislinger, T. (2014). The proteomics of prostate cancer exosomes. *Expert Review of Proteomics*. *11*, 167–177. https://doi.org/10.1586/14789450.2014.890894

Drake, R. R., White, K. Y., Fuller, T. W., Igwe, E., Clements, M. A., Nyalwidhe, J. O., Given, R. W., Lance, R. S., & Semmes, O. J.(2009). Clinical collection and protein properties of expressed prostatic secretions as a source for biomarkers of prostatic disease. *Journal of Proteomics*, *72*, 907–917. https://doi.org/10.1016/j.jprot.2009.01.007

Duffy, M. J. (2020). Biomarkers for prostate cancer: Prostate-specific antigen and beyond. *Clinical Chemistry and Laboratory Medicine*, *58*, 326–339. https://doi.org/10.1515/cclm-2019-0693

Duijvesz, D., Luider, T., Bangma, C. H., & Jenster, G. (2011). Exosomes as biomarker treasure chests for prostate cancer. *European Urology*, *59*, 823–831. https://doi.org/10.1016/j.eururo.2010.12.031

Emmanouilidou, E., Melachroinou, K., Roumeliotis, T., Garbis, S. D., Ntzouni, M., Margaritis, L. H., Stefanis, L., & Vekrellis, K. (2010). Cell-produced alpha-synuclein is secreted in a calcium-dependent manner by exosomes and impacts neuronal survival. *Journal of Neuroscience*, *30*, 6838-6851. https://doi.org/10.1523/JNEUROSCI.5699-09.2010

Erdbrügger, U., Blijdorp, C. J., Bijnsdorp, I. V., Borràs, F. E., Burger, D., Bussolati, B., Byrd, J. B., Clayton, A., Dear, J. W., Falcón-Pérez, J. M., Grange, C., Hill, A. F., Holthöfer, H., Hoorn, E. J., Jenster, G., Jimenez, C. R., Junker, K., Klein, J., Knepper, M. A., Koritzinsky, E. H., Luther, J. M., … Martens-Uzunova, E. S. (2021). Urinary extracellular vesicles: A position paper by the Urine Task Force of the International Society for Extracellular Vesicles. *Journal of Extracellular Vesicles*, *10*. https://doi.org/10.1002/jev2.12093

Fernández-Llama, P., Khositseth, S., Gonzales, P. A., Star, R. A., Pisitkun, T., & Knepper, M. A. (2010). Tamm-Horsfall protein and urinary exosome isolation. *Kidney International*, *77*, 736–742. https://doi.org/10.1038/ki.2009.550

Fujiki, Y., Fowler, S., Shio, H., Hubbard, A. L., & Lazarow, P. B. (1982). Polypeptide and phospholipid composition of the membrane of rat liver peroxisomes: Comparison with endoplasmic reticulum and mitochondrial membranes. *Journal of Cell Biology*, *93*, 103–110. https://doi.org/10.1083/jcb.93.1.103

Fujiki, Y., Hubbard, A. L., Fowler, S., & Lazarow, P. B. (1982). Isolation of intracellular membranes by means of sodium carbonate treatment: Application to endoplasmic reticulum. *Journal of Cell Biology*, *93*, 97–102. https://doi.org/10.1083/jcb.93.1.97

Fujita, K., Kume, H., Matsuzaki, K., Kawashima, A., Ujike, T., Nagahara, A., Uemura, M., Miyagawa, Y., Tomonaga, T., & Nonomura, N. (2017). Proteomic analysis of urinary extracellular vesicles from high Gleason score prostate cancer. *Scientific Reports*, *7*, 42961. https://doi.org/10.1038/srep42961

Gardiner, C., Di Vizio, D., Sahoo, S., Théry, C., Witwer, K. W., Wauben, M., & Hill, A. F. (2016). Techniques used for the isolation and characterization of extracellular vesicles: Results of a worldwide survey. *Journal of Extracellular Vesicles*, *5*, 32945. https://doi.org/10.3402/jev.v5.32945

Gonzales, P. A., Pisitkun, T., Hoffert, J. D., Tchapyjnikov, D., Star, R. A., Kleta, R., Wang, N. S., & Knepper, M. A. (2009). Large-scale proteomics and phosphoproteomics of urinary exosomes. *Journal of the American Society of Nephrology*, *20*, 363-379. https://doi.org/10.1681/ASN.2008040406

Hessvik, N. P., & Llorente, A. (2018). Current knowledge on exosome biogenesis and release. *Cellular and Molecular Life Sciences*, *75*, 193–208. https://doi.org/10.1007/s00018-017-2595-9

Hiemstra, T. F., Charles, P. D., Hester, S. S., Karet, F. E., & Lilley, K. S. (2011). Uromodulin exclusion list improves urinary exosomal protein identification. *Journal of Biomolecular Techniques*, *22*, 136–145.

Hu, Q., Su, H., Li, J., Lyon, C., Tang, W., Wan, M., & Hu, T. Y. (2020). Clinical applications of exosome membrane proteins. *Precision Clinical Medicine*, *3*, 54–66. https://doi.org/10.1093/pcmedi/pbaa007

Jang, S. C., Crescitelli, R., Cvjetkovic, A., Belgrano, V., Olofsson Bagge, R., Sundfeldt, K., Ochiya, T., Kalluri, R., & Lötvall, J. (2019). Mitochondrial protein enriched extracellular vesicles discovered in human melanoma tissues can be detected in patient plasma. *Journal of Extracellular Vesicles*, *8*, 1635420. https://doi.org/10.1080/20013078.2019.1635420

Jeon, J., Olkhov-Mitsel, E., Xie, H., Yao, C. Q., Zhao, F., Jahangiri, S., Cuizon, C., Scarcello, S., Jeyapala, R., Watson, J. D., Fraser, M., Ray, J., Commisso, K., Loblaw, A., Fleshner, N. E., Bristow, R. G., Downes, M., Vesprini, D., Liu, S., Bapat, B., & Boutros, P. C. (2020). Temporal stability and prognostic biomarker potential of the prostate cancer urine miRNA transcriptome. *JNCI Journal of the National Cancer Institute*, *112*, 247–255. https://doi.org/10.1093/jnci/djz112

Jeppesen, D. K., Nawrocki, A., Jensen, S. G., Thorsen, K., Whitehead, B., Howard, K. A., Dyrskjøt, L., Ørntoft, T. F., Larsen, M. R. & Ostenfeld, M. S. (2014). Quantitative proteomics of fractionated membrane and lumen exosome proteins from isogenic metastatic and nonmetastatic bladder cancer cells reveal differential expression of EMT factors. *Proteomics*, *14*, 699–712. https://doi.org/10.1002/pmic.201300452

Kaiser, W. J., Holbrook, L.-M., Tucker, K. L., Stanley, R. G., & Gibbins, J. M. (2009). A functional proteomic method for the enrichment of peripheral membrane proteins reveals the collagen binding protein Hsp47 is exposed on the surface of activated human platelets. *Journal of Proteome Research*, *8*, 2903–2914. https://doi.org/10.1021/pr900027j

Kalra, H., Simpson, R. J., Ji, H., Aikawa, E., Altevogt, P., Askenase, P., Bond, V. C., Borràs, F. E., Breakefield, X., Budnik, V., Buzas, E., Camussi, G., Clayton, A., Cocucci, E., Falcon-Perez, J. M., Gabrielsson, S., Gho, Y. S., Gupta, D., Harsha, H. C., & Hendrix, An, … Mathivanan, S. (2012). Vesiclepedia: A compendium for extracellular vesicles with continuous community annotation. *PLOS Biology*, *10*, e1001450. https://doi.org/10.1371/journal.pbio.1001450

Karasu, E., Eisenhardt, S. U., Harant, J., & Huber-Lang, M. (2018). Extracellular vesicles: Packages sent with complement. *Frontiers in Immunology*, *9*. https://doi.org/10.3389/fimmu.2018.00721

Keerthikumar, S., Chisanga, D., Ariyaratne, D., Al Saffar, H., Anand, S., Zhao, K., Samuel, M., Pathan, M., Jois, M., Chilamkurti, N., Gangoda, L., & Mathivanan, S. (2016). ExoCarta: A web-based compendium of exosomal cargo. *Journal of Molecular Biology*, *428*, 688–692. https://doi.org/10.1016/j.jmb.2015.09.019

Kim, H., Botelho, S. C., Park, K., & Kim, H. (2015). Use of carbonate extraction in analyzing moderately hydrophobic transmembrane proteins in the mitochondrial inner membrane. *Protein Science*, *24*, 2063–2069. https://doi.org/10.1002/pro.2817

Kim, Y., Jeon, J., Mejia, S., Yao, C. Q., Ignatchenko, V., Nyalwidhe, J. O., Gramolini, A. O., Lance, R. S., Troyer, D. A., Drake, R. R., Boutros, P. C., Semmes, O. J., & Kislinger, T. (2016). Targeted proteomics identifies liquid-biopsy signatures for extracapsular prostate cancer. *Nature Communications*, *7*, 11906. https://doi.org/10.1038/ncomms11906

Ko, S. Y., & Naora, H. (2020). Extracellular vesicle membrane-associated proteins: Emerging roles in tumor angiogenesis and anti-angiogenesis therapy resistance. *International Journal of Molecular Sciences*, *21*, 5418. https://doi.org/10.3390/ijms21155418

Kosanović, M., & Janković, M. (2014). Isolation of urinary extracellular vesicles from Tamm-Horsfall protein–Depleted urine and their application in the development of a lectin-exosome-binding assay. *Biotechniques*, *57*, 143–149. https://doi.org/10.2144/000114208

Kowal, J., Tkach, M., & Théry, C. (2014). Biogenesis and secretion of exosomes. *Current Opinion in Cell Biology*, *29*, 116–125. https://doi.org/10.1016/j.ceb.2014.05.004

Liang, Y., Lehrich, B. M., Zheng, S., & Lu, M. (2021). Emerging methods in biomarker identification for extracellular vesicle-based liquid biopsy. *Journal of Extracellular Vesicles*, *10*. https://doi.org/10.1002/jev2.12090

Litwin, M. S., & Tan, H.-J. (2017). The diagnosis and treatment of prostate cancer. *JAMA*, *317*(24), 2532–2542. https://doi.org/10.1001/jama.2017.7248

Liu, X., Yu, X., Zack, D. J., Zhu, H., & Qian, J. (2008). TiGER: A database for tissue-specific gene expression and regulation. *BMC Bioinformatics*, *9*, 1–7. https://doi.org/10.1186/1471-2105-9-271

Liu, Z., Cauvi, D. M., Bernardino, E. M. A., Lara, B., Lizardo, R. E., Hawisher, D., Bickler, S., & De Maio, A. (2018). Isolation and characterization of human urine extracellular vesicles. *Cell Stress Chaperones*, *23*, 943–953. https://doi.org/10.1007/s12192-018-0902-5

Micanovic, R., Lafavers, K., Garimella, P. S., Wu, X.-R., & El-Achkar, T. M. (2020). Uromodulin (Tamm-Horsfall protein): Guardian of urinary and systemic homeostasis. *Nephrology Dialysis Transplantation*, *35*, 33–43. https://doi.org/10.1093/ndt/gfy394

Murphy, D. E., De Jong, O. G., Brouwer, M., Wood, M. J., Lavieu, G., Schiffelers, R. M., & Vader, P. (2019). Extracellular vesicle-based therapeutics: Natural versus engineered targeting and trafficking. *Experimental & Molecular Medicine*, *51*, 32. https://doi.org/10.1038/s12276-019-0223-5

Musante, L., Bontha, S. V., La Salvia, S., Fernandez-Piñeros, A., Lannigan, J., Le, T. H., Mas, V., & Erdbrügger, U. (2020). Rigorous characterization of urinary extracellular vesicles (uEVs) in the low centrifugation pellet - a neglected source for uEVs. *Scientific Reports*, *10*(1), https://doi.org/10.1038/s41598-020-60619-w

Musante, L., Saraswat, M., Duriez, E., Byrne, B., Ravidà, A., Domon, B., Holthofer, H. (2012). Biochemical and physical characterisation of urinary nanovesicles following CHAPS treatment. *PLoS One*, *7*, e37279. https://doi.org/10.1371/journal.pone.0037279

Nawaz, M., Camussi, G., Valadi, H., Nazarenko, I., Ekström, K., Wang, X., Principe, S., Shah, N., Ashraf, N. M., Fatima, F., Neder, L., & Kislinger, T. (2014). The emerging role of extracellular vesicles as biomarkers for urogenital cancers. *Nature Reviews Urology*, *11*, 688–701. https://doi.org/10.1038/nrurol.2014.301

Oeyen, E., Willems, H., 'T Kindt, R., Sandra, K., Boonen, K., Hoekx, L., De Wachter, S., Ameye, F., & Mertens, I. (2019). Determination of variability due to biological and technical variation in urinary extracellular vesicles as a crucial step in biomarker discovery studies. *Journal of Extracellular Vesicles*, *8*, 1676035 https://doi.org/10.1080/20013078.2019.1676035

Øverbye, A., Skotland, T., Koehler, C. J., Thiede, B., Seierstad, T., Berge, V., Sandvig, K., & Llorente, A. (2015). Identification of prostate cancer biomarkers in urinary exosomes. *Oncotarget*, *6*, 30357–30376. doi:10.18632/oncotarget.4851

Palmisano, G., Jensen, S. S., Le Bihan, M.-C., Lainé, J., McGuire, J. N., Pociot, F., & Larsen, M. R. (2012). Characterization of Membrane-shed Microvesicles from Cytokine-stimulated β-Cells Using Proteomics Strategies. *Molecular & Cellular Proteomics*, *11*(8), 230–243. https://doi.org/10.1074/mcp.m111.012732

Palviainen, M., Saraswat, M., Varga, Z., Kitka, D., Neuvonen, M., Puhka, M., Joenväärä, S., Renkonen, R., Nieuwland, R., Takatalo, M., & Siljander, P. R. M. (2020). Extracellular vesicles from human plasma and serum are carriers of extravesicular cargo—Implications for biomarker discovery. *PLoS One*, *15*, e0236439. https://doi.org/10.1371/journal.pone.0236439

Perez-Riverol, Y., Csordas, A., Bai, J., Bernal-Llinares, M., Hewapathirana, S., Kundu, D. J., Inuganti, A., Griss, J., Mayer, G., Eisenacher, M., Pérez, E., Uszkoreit, J., Pfeuffer, J., Sachsenberg, T., Yılmaz, Ş., Tiwary, S., Cox, J., Audain, E., Walzer, M., Jarnuczak, A. F., Ternent, T., Brazma, A., & Vizcaíno, J. A. (2019). The PRIDE database and related tools and resources in 2019: Improving support for quantification data. *Nucleic Acids Research*, *47*, D442–D450. https://doi.org/10.1093/nar/gky1106

Pisitkun, T., Shen, R. F., & Knepper, M. A. (2004). Identification and proteomic profiling of exosomes in human urine. *Proceedings of the National Academy of Sciences of the United States of America*, *101*, 13368–13373. https://doi.org/10.1073/pnas.0403453101

Principe, S., Jones, E. E., Kim, Y., Sinha, A., Nyalwidhe, J. O., Brooks, J., Semmes, O. J., Troyer, D. A., Lance, R. S., Kislinger, T., & Drake, R. R. (2013). In-depth proteomic analyses of exosomes isolated from expressed prostatic secretions in urine. *Proteomics*, *13*, 1667–1671. https://doi.org/10.1002/pmic.201200561

Principe, S., Kim, Y., Fontana, S., Ignatchenko, V., Nyalwidhe, J. O., Lance, R. S., Troyer, D. A., Alessandro, R., Semmes, O. J., Kislinger, T., Drake, R. R., & Medin, J. A. (2012). Identification of prostate-enriched proteins by in-depth proteomic analyses of expressed prostatic secretions in urine. *Journal of Proteome Research*, *11*, 2386–2396. https://doi.org/10.1021/pr2011236

Puhka, M., Nordberg, M. E., Valkonen, S., Rannikko, A., Kallioniemi, O., Siljander, P., & Af Hällström, T. M. (2017). KeepEX, a simple dilution protocol for improving extracellular vesicle yields from urine. *European Journal of Pharmaceutical Sciences*, *98*, 30–39. https://doi.org/10.1016/j.ejps.2016.10.021

Purushothaman, A., Bandari, S. K., Liu, J., Mobley, J. A., Brown, E. E., & Sanderson, R. D. (2016). Fibronectin on the surface of myeloma cell-derived exosomes mediates exosome-cell interactions. *Journal of Biological Chemistry*, *291*, 1652–1663. https://doi.org/10.1074/jbc.M115.686295

Raposo, G., & Stoorvogel, W. (2013). Extracellular vesicles: Exosomes, microvesicles, and friends. *Journal of Cell Biology*, *200*, 373-383. https://doi.org/10.1083/jcb.201211138

Raudvere, U., Kolberg, L., Kuzmin, I., Arak, T., Adler, P., Peterson, H., & Vilo, J. (2019). g:Profiler: A web server for functional enrichment analysis and conversions of gene lists (2019 update). *Nucleic Acids Research*, *47*, W191–W198. https://doi.org/10.1093/nar/gkz369

Reimand, J., Isserlin, R., Voisin, V., Kucera, M., Tannus-Lopes, C., Rostamianfar, A., Wadi, L., Meyer, M., Wong, J., Xu, C., Merico, D., & Bader, G. D. (2019). Pathway enrichment analysis and visualization of omics data using g:Profiler, GSEA, Cytoscape and EnrichmentMap. *Nature Protocols*, *14*, 482–517. https://doi.org/10.1038/s41596-018-0103-9

Rieu, S., Géminard, C., Rabesandratana, H., Sainte-Marie, J., & Vidal, M. (2000). Exosomes released during reticulocyte maturation bind to fibronectin via integrin $\alpha 4\beta 1$. *European Journal of Biochemistry*, *267*, 583–590. https://doi.org/10.1046/j.1432-1327.2000.01036.x

Rood, I. M., Deegens, J. K. J., Merchant, M. L., Tamboer, W. P. M., Wilkey, D. W., Wetzels, J. F. M., & Klein, J. B. (2010). Comparison of three methods for isolation of urinary microvesicles to identify biomarkers of nephrotic syndrome. *Kidney International*, *78*, 810–816. https://doi.org/10.1038/ki.2010.262

Rosa-Fernandes, L., Rocha, V. B., Carregari, V. C., Urbani, A., & Palmisano, G. (2017). A perspective on extracellular vesicles proteomics. *Frontiers in Chemistry*, *5*, 102. https://doi.org/10.3389/fchem.2017.00102

Royo, F., Théry, C., Falcón-Pérez, J. M., Nieuwland, R., & Witwer, K. W. (2020). Methods for separation and characterization of extracellular vesicles: Results of a worldwide survey performed by the ISEV rigor and standardization subcommittee. *Cells*, *9*, 1955. https://doi.org/10.3390/cells9091955

Ruan, Y., Pei, W., & Wan, M. (2008). Membrane protein analysis of human breast cancer cell line MCF-7 by different membrane washing methods. *Cell Biochemistry & Function*, *26*, 787–796. https://doi.org/10.1002/cbf.1507

Säemann, M. D., Weichhart, T., Zeyda, M., Staffler, G., Schunn, M., Stuhlmeier, K. M., Sobanov, Y., Stulnig, T. M., Akira, S., Von Gabain, A., Von Ahsen, U., Hörl, W. H., & Zlabinger, G. J. (2005). Tamm-Horsfall glycoprotein links innate immune cell activation with adaptive immunity via a Toll-like receptor-4–dependent mechanism. *Journal of Clinical Investigation*, *115*, 468–475. https://doi.org/10.1172/JCI22720

Santucci, L., Bruschi, M., Del Zotto, G., Antonini, F., Ghiggeri, G., M., Panfoli, I., & Candiano, G. (2019). Biological surface properties in extracellular vesicles and their effect on cargo proteins. *Scientific Reports*, *9*, 1–12. https://doi.org/10.1038/s41598-019-47598-3

Siegel, R. L., Miller, K. D., Fuchs, H. E., & Jemal, A. (2021). Cancer statistics, 2021. *CA: A Cancer Journal for Clinicians*, *71*, 7–33. https://doi.org/10.3322/caac.21654

Simonsen, J. B., & Münter, R. (2020). Pay attention to biological nanoparticles when studying the protein corona on nanomedicines. *Angewandte Chemie International Edition*, *59*, 12584–12588. https://doi.org/10.1002/anie.202004611

Sung, B. H., Ketova, T., Hoshino, D., Zijlstra, A., & Weaver, A. M. (2015). Directional cell movement through tissues is controlled by exosome secretion. *Nature Communications*, *6*, 7164. https://doi.org/10.1038/ncomms8164

Théry, C., Clayton, A., Amigorena, S., & Raposo, G. (2006). Isolation and characterization of exosomes from cell culture supernatants. *Current Protocols in Cell Biology*. https://doi.org/10.1002/0471143030.cb0322s30

Théry, C., Witwer, K. W., Aikawa, E., Alcaraz, M. J., Anderson, J. D., Andriantsitohaina, R., Antoniou, A., Arab, T., Archer, F., Atkin-Smith, G. K., Ayre, D. C., Bach, J.-M., Bachurski, D., Baharvand, H., Balaj, L., Baldacchino, S., Bauer, N. N., Baxter, A. A., Bebawy, M., Beckham, C., Bedina Zavec, A., Benmoussa, A., Berardi, A. C., Bergese, P., … Zuba-Surma, E. K. (2018). Minimal information for studies of extracellular vesicles 2018 (MISEV2018): A position statement of the International Society for Extracellular Vesicles and update of the MISEV2014 guidelines. *Journal of Extracellular Vesicles*, *7*, 1535750. https://doi.org/10.1080/20013078.2018.1535750

Tyanova, S., & Cox, J. (2018). Perseus: A bioinformatics platform for integrative analysis of proteomics data in cancer research. In von Stechow, L. (Eds.), *Cancer Systems Biology. Methods in Molecular Biology* (Vol. 1711, pp. 133–148). New York, NY: Humana Press. https://doi.org/10.1007/978-1-4939-7493-1_7

Uhlén, M., Fagerberg, L., Hallström, B. M., Lindskog, C., Oksvold, P., Mardinoglu, A., Sivertsson, Å., Kampf, C., Sjöstedt, E., Asplund, A., Olsson, I., Edlund, K., Lundberg, E., Navani, S., Szigyarto, C. A., Odeberg, J., Djureinovic, D., Takanen, J. O., Hober, S., Alm, T., Edqvist, P.-H., … Pontén, F. (2015). Tissue-based map of the human proteome. *Science*, *347*, 1260419–1260419. https://doi.org/10.1126/science.1260419

Van Deun, J., Mestdagh, P., Agostinis, P., Akay, Ö., Anand, S., Anckaert, J., Martinez, Z. A., Baetens, T., Beghein, E., Bertier, L., Berx, G., Boere, J., Boukouris, S., Bremer, M., Buschmann, D., Byrd, J. B., Casert, C., Cheng, L., Cmoch, A., Daveloose, D., De Smedt, E., Demirsoy, S., … Hendrix, A. (2017). EV-TRACK: Transparent reporting and centralizing knowledge in extracellular vesicle research. *Nature Methods*, *14*, 228–232. https://doi.org/10.1038/nmeth.4185

Véron, P., Segura, E., Sugano, G., Amigorena, S., & Théry, C. (2005). Accumulation of MFG-E8/lactadherin on exosomes from immature dendritic cells. *Blood Cells, Molecules and Diseases*, *35*, 81–88. https://doi.org/10.1016/j.bcmd.2005.05.001

Wachalska, M., Koppers-Lalic, D., Van Eijndhoven, M., Pegtel, M., Geldof, A. A., Lipinska, A. D., Van Moorselaar, R. J., & Bijnsdorp, I. V. (2016). Protein complexes in urine interfere with extracellular vesicle biomarker studies. *Journal of Circulating Biomarkers*, *5*, 1–6. https://doi.org/10.5772/62579

Wang, Z., Hill, S., Luther, J. M., Hachey, D. L., & Schey, K. L. (2012). Proteomic analysis of urine exosomes by multidimensional protein identification technology (MudPIT). *Proteomics*, *12*, 329–338. https://doi.org/10.1002/pmic.201100477

Webber, J., & Clayton, A. (2013). How pure are your vesicles? *Journal of Extracellular Vesicles*, *2*, 19861. https://doi.org/10.3402/jev.v2i0.19861

Wiggins, R. C. (1987). Uromucoid (Tamm-Horsfall glycoprotein) forms different polymeric arrangements on a filter surface under different physicochemical conditions. *Clinica Chimica Acta*, *162*, 329–340. https://doi.org/10.1016/0009-8981(87)90052-0

Wu, T.-H., Li, K.-J., Yu, C.-L., & Tsai, C.-Y. (2018). Tamm–Horsfall protein is a potent immunomodulatory molecule and a disease biomarker in the urinary system. *Molecules*, *23*(1), 200. https://doi.org/10.3390/molecules23010200

Xu, R., Greening, D. W., Chen, M., Rai, A., Ji, H., Takahashi, N., & Simpson, R. J. (2019). Surfaceome of exosomes secreted from the colorectal cancer cell line SW480: Peripheral and integral membrane proteins analyzed by proteolysis and TX114. *Proteomics*, *19*, 1700453. https://doi.org/10.1002/pmic.201700453

Xu, X., Barreiro, K., Musante, L., Kretz, O., Lin, H., Zou, H., Huber, T. B., & Holthofer, H. (2019). Management of Tamm–Horsfall protein for reliable urinary analytics. *PROTEOMICS – Clinical Applications*, *13*, 1–10. https://doi.org/10.1002/prca.201900018

Yang, L., Dutta, S. M., Troyer, D. A., Lin, J. B., Lance, R. A., Nyalwidhe, J. O., Drake, R. R., & Semmes, O. J. (2015). Dysregulated expression of cell surface glycoprotein CDCP1 in prostate cancer. *Oncotarget*, *6*, 43743–43758. doi:10.18632/oncotarget.6193

Yang, L., Nyalwidhe, J. O., Guo, S., Drake, R. R., & Semmes, O. J. (2011). Targeted identification of metastasis-associated cell-surface sialoglycoproteins in prostate cancer. *Molecular & Cellular Proteomics*, *10*, M110.007294. https://doi.org/10.1074/mcp.M110.007294

Zhou, H., Yuen, P. S. T., Pisitkun, T., Gonzales, P. A., Yasuda, H., Dear, J. W., Gross, P., Knepper, M. A., & Star, R. A. (2006). Collection, storage, preservation, and normalization of human urinary exosomes for biomarker discovery. *Kidney International*, *69*, 1471–1476. https://doi.org/10.1038/sj.ki.5000273

Zhu, Y., Lim, W., Tan, B., Teo, T., & Duan, W. (2005). Identification of an integral plasma membrane pool of protein kinase C in mammalian tissues and cells. *Cellular Signalling*, *17*, 1125-1136. https://doi.org/10.1016/j.cellsig.2004.12.004

SUPPORTING INFORMATION

Additional supporting information may be found in the online version of the article at the publisher's website.

How to cite this article: Correll, V. L., Otto, J. J., Risi, C. M., Main, B. P., Boutros, P. C., Kislinger, T., Galkin, V. E., Nyalwidhe, J. O., Semmes, O. J., & Yang, L. (2022). Optimization of small extracellular vesicle isolation from expressed prostatic secretions in urine for in-depth proteomic analysis. *Journal of Extracellular Vesicles*, *11*, e12184. https://doi.org/10.1002/jev2.12184